EUROPEAN ORGANIZATION FOR NUCLEAR RESEARCH
CERN - ACCELERATORS AND TECHNOLOGY SECTOR

CERN-ATS-2013-019

Superconducting Magnets for Particle Accelerators

L. Rossi, L. Bottura

Superconductivity has been the most influential technology in the field of accelerators in the last 30 years. Since the commissioning of the Tevatron, which demonstrated the use and operability of superconductivity on a large scale, superconducting magnets and rf cavities have been at the heart of all new large accelerators. Superconducting magnets have been the invariable choice for large colliders, as well as cyclotrons and large synchrotrons. In spite of the long history of success, superconductivity remains a difficult technology, requires adequate R&D and suitable preparation, and has a relatively high cost. Hence, it is not surprising that the development has also been marked by a few setbacks. This article is a review of the main superconducting accelerator magnet projects; it highlights the main characteristics and main achievements, and gives a perspective on the development of superconducting magnets for the future generation of very high energy colliders.

To be published in Reviews of Accelerator Science and Technology, Vol. 5

Geneva, Switzerland

February 2013

Reviews of Accelerator Science and Technology
Vol. 5 (2012) 51–89

DOI: 10.1142/S1793626812300034

World Scientific
www.worldscientific.com

Superconducting Magnets for Particle Accelerators

Lucio Rossi
CERN, Technology Department,
Genève 23, CH-1211, Switzerland
lucio.rossi@cern.ch

Luca Bottura
CERN, Technology Department, Magnet Group Leader,
Genève 23, CH-1211, Switzerland
luca.bottura@cern.ch

Superconductivity has been the most influential technology in the field of accelerators in the last 30 years. Since the commissioning of the Tevatron, which demonstrated the use and operability of superconductivity on a large scale, superconducting magnets and rf cavities have been at the heart of all new large accelerators. Superconducting magnets have been the invariable choice for large colliders, as well as cyclotrons and large synchrotrons. In spite of the long history of success, superconductivity remains a difficult technology, requires adequate R&D and suitable preparation, and has a relatively high cost. Hence, it is not surprising that the development has also been marked by a few setbacks. This article is a review of the main superconducting accelerator magnet projects; it highlights the main characteristics and main achievements, and gives a perspective on the development of superconducting magnets for the future generation of very high energy colliders.

Keywords: Superconductivity; magnets; accelerators; large scale applied superconductivity.

1. Introduction

In the same year in which he received the Nobel Prize for the investigation of properties of matter at low temperature (we can certainly say superconductivity is the most striking part of it!), K. H. Onnes [1] was dreaming of a 100,000 G (10 T) magnet. However, it took much more time than he thought for the dream to become a reality, and only at the end of the 1970s did superconducting magnet technology really take off. From then on, magnets have been the most important application of superconductivity, and accelerators can be credited with being among the drivers of the development of this technology.

One characteristic of accelerators is that they are pursued by large laboratories, with programs over a long time, which allows investigation and R&D to be done in a fruitful way. The latest example, the LHC, is the summit of over 30 years of development of superconducting magnets (SCMs). Its giant size and its outspoken goals — the Higgs particle, whose recent discovery [2] has been heralded worldwide, and the unveiling of the new world beyond the Standard Model — make the LHC the crossroads between past and future R&D.

2. Main Characteristics of Superconducting Magnets for Accelerators

Magnets are different according to the type of accelerators they are intended for. Colliders or synchrotrons for high energy physics (HEP) rings are the most challenging and they are superconducting with a few exceptions, such as fast cycling machines (for example, the J-PARC main ring). Magnets for superconducting linear colliders, such as the ILC or X-FEL, are also superconducting, a choice mainly motivated by the advantage of integration with the superconducting radio-frequency (SCRF) cavities, rather than by technical gain. Finally, there is a considerable effort in the development of SCMs for low energy accelerators, like cyclotrons or synchro-cyclotrons. These were used in the past mainly for nuclear research but are now mainly for medical

applications. This type of SCM is akin to magnets for particle detector spectrometry or for MRI. In this article we will consciously restrict the scope to SCMs for HEP colliders.

SCMs become of interest when the required field is above the iron saturation limit, i.e. approximately 2 T. In some instances, however, SCMs are becoming the preferred choice for their compactness and their low energy consumption, a topic that is increasingly important in the design of new accelerators.

2.1. *Functions of superconducting magnets*

The first function of a magnet is to guide and steer the particle, i.e. to keep it in orbit in a circular accelerator or to just bend in a transfer line. The second main function is focusing the beam, thus providing it with the necessary stability in the plane perpendicular to the trajectory.

Except when the beam has a very low energy, a domain where solenoids are suitable, the adequate force can be given only by a transverse field, i.e. a magnetic field perpendicular to the particle trajectory. In the case of high energy accelerators, like synchrotrons and colliders, the beam region is a cylinder that follows the beam path and has the smallest practical dimension, as shown in Fig. 1. As will be discussed later, the cost and technical complexity of the magnetic system are proportional to the energy stored in the magnetic field, which explains why it is important to minimize the size of the magnet bore.

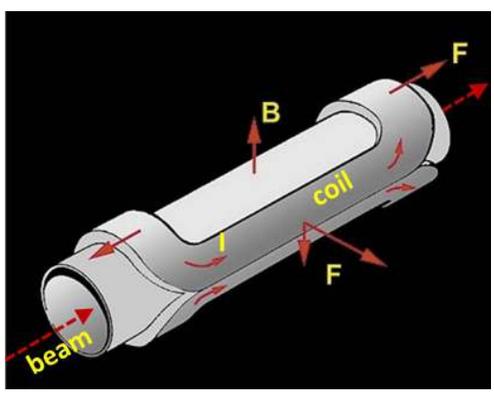

Fig. 1. Schematic of an accelerator dipole.

Despite the fact that static magnetic fields do not accelerate, in circular accelerators the bending (dipole) field eventually determines the final energy reach. In relativistic conditions, the relation between the beam energy, E_{beam} (in TeV), the dipole field B (in T) and the radius of the beam trajectory inside the bending field R (in km) takes a very simple form:

$$E_{\mathrm{beam}} \cong 0.3BR. \tag{1}$$

Since the dipole field typically covers two-thirds of the accelerator, R is about two-thirds of the average radius of the ring. Equation (1) shows clearly the interest in the highest possible field for a given tunnel.

The other important function of magnets is, in general terms, to assure the stability of the beam in the transverse space. This is accomplished by quadrupoles, sextupoles and octupoles. While the main quadrupoles are usually of similar — although reduced — size and complexity with respect to the main dipoles, sextupoles and octupoles are of much smaller size and field. In this context it is worth mentioning the quadrupoles that are just before the collision points. These quadrupoles, usually called low-β, provide the optical manipulation to focus the beam to the smallest feasible dimension (the minimum β function) at the collision point. This set of quadrupoles features an aperture significantly larger than the lattice quadrupoles, and requires a large field gradient, which results in a peak field that can be close to that of the main dipoles.

A key demand on accelerator magnets is good field quality: the harmonic content of main magnets and low-β triplet quadrupoles needs to be designed, controlled during production and corrected in operation to a precision of 10–100 ppm. Given the unavoidable manufacturing tolerances and uncertainties, this implies extensive use of corrector magnets. Small dipole correctors are needed to maintain the beam on the desired orbit or to generate local bumps. Higher order corrector magnets, of small size and in great numbers, are distributed all over the ring to trim the linear beam parameters such as tune and chromaticity, and insure nonlinear stability. As an example, in the LHC there are almost 8000 superconducting corrector magnets from dipoles up to dodecapoles (12-pole), distributed all over the ring.

2.2. *Magnet design*

The design of superconducting accelerator magnets is largely concerned with the optimal distribution of compact superconductors around the beam aperture. In fact, in contrast to classical electromagnets, the field in a superconducting accelerator magnet is mainly produced by the current in the conductor, rather than the magnetization of an iron yoke. Very schematically, an SCM for large scale accelerators consists of a coil wound with highly compacted cables, tightly packed around the bore which delimits the vacuum chamber hosting the beam. The coil shape is optimized to maximize the bore field and achieve acceptable field quality, as described later. The large forces that are experienced by the coil (several tens to hundreds of tons per meter) cannot be reacted by the winding alone, which has the characteristic shape of a slender racetrack (see Fig. 1), and hence the force is transferred to a structure that guarantees mechanical stability and rigidity. The iron yoke that surrounds this assembly closes the magnetic circuit, shielding the surroundings from stray fields and providing a marginal gain of magnetic field in the bore. In addition, it can have a structural function in reacting or transferring the Lorentz forces from the coil to an external cylinder. Finally, the magnet is enclosed in a cryostat that provides the thermal barrier features necessary for cooling the magnet to the operating temperature, which is in the cryogenic range (1.9–4.5 K for accelerators built to date). Various implementations of this basic concept are discussed in the review of the historical development of accelerator magnets (see Sec. 3), while in Fig. 2 the cross section of the LHC dipole in its cryostat illustrates this principle.

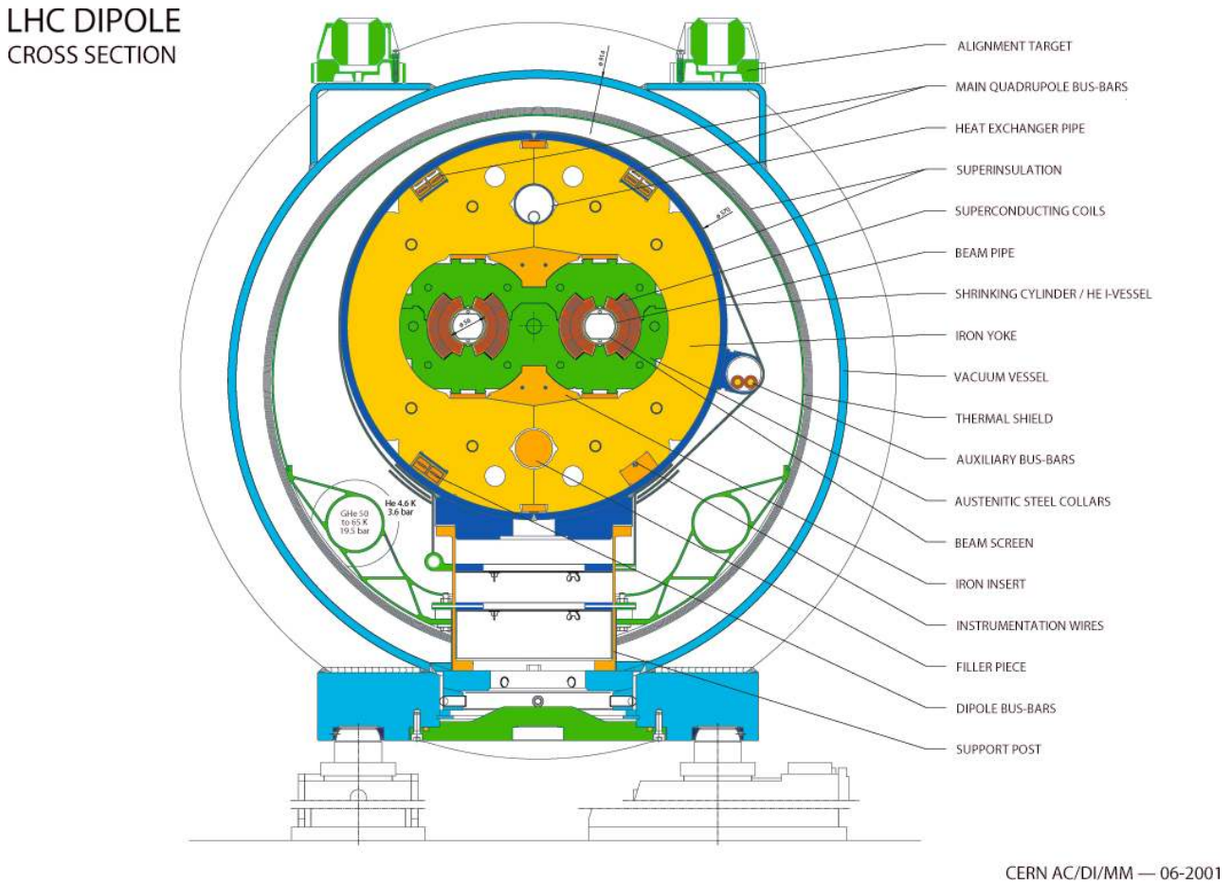

Fig. 2. Cross section of the LHC dipole in its cryostat.

2.2.1. *Electromagnetic design*

The prime purpose of the electromagnetic design is to obtain a multipolar field with the quality demanded by beam physics requirements. For long and slender HEP magnets, the magnetic field is 2D and is best represented using complex multipoles [3]. Defining the complex variable $z = x + iy$, where the plane (x, y) is that of the magnet cross section, the function $B_y + iB_x$ of the two components of the magnetic field is expanded in series:

$$B_y + iB_x = \sum_{n=1}^{\infty} (B_n + iA_n) z^{n-1}. \qquad (2)$$

The coefficients B_n and A_n of the series expansion, called normal and skew components respectively, are the multipoles of the field, and determine the shape of the field lines. A pure multipolar field has only one nonzero B_n(or A_n) for a given value of n, which is called the main order of the field. As an example, $n = 1$ is a pure dipole and $n = 2$ is a quadrupole. Nonzero B_n and A_n for n other than the main order are usually referred to as *field harmonics* or *field errors*.

Several ways can be found to generate perfect multipolar fields required by HEP accelerator magnets. As an example, we show in Fig. 3 a number of arrangements of current distribution that generates a perfect transverse dipole field. It has been demonstrated by I. Rabi [4] that two uniform current density cylinders with opposite current polarity generate a perfect dipole field in the region of current overlap, i.e. in the internal current-free region.

The total surface current, $J_s = J \cdot t$, J being the current density and t the current thickness at the midplane, is maximum at the midplane and zero at the vertical axis, following a $\cos\vartheta$ behavior. More generally, the uniform dipole field may be generated by a constant current density with a geometry given by opposite intersecting ellipses. The current distribution obtained with two overlapping ellipses, rotated by 90°, produces a quadrupole field. In the above cases the region of the intersection cannot be a circle.

As an alternative, a perfect dipole field can be generated by a shell of current, of constant thickness t, in which the volume current density is maximum at the midplane and vanishes toward the pole region with a $J = J_0 \cos\vartheta$ dependence. In this case the inner region can be perfectly circular. A $J_0 \cos\vartheta$ not only generates a perfect dipole field, but is the most efficient current distribution, i.e. any other distribution requires more total current (Ampère turns) to generate a given central field; it produces more magnetic flux and has higher stored energy. This consideration is very important for SCMs for which the cost of the conductor is one of the dominant cost factors. It is instructive to compare the central field of the dipole generated by the ideal $\cos\vartheta$ distribution, $B_0 = 1/2\mu_0 J_0 t$, to that of an infinitely long solenoid of the same current density and thickness, i.e. $B_0 = \mu_0 J_0 t$. In practice, the same current density and thickness generates only half the field of the solenoid configuration: what in a solenoid is a moderate field level can be considered a great achievement for transverse field magnets!

As with the dipole, a perfect quadrupole field can be generated by a thin shell of constant thickness with a current density varying as $J = J_0 \cos 2\vartheta$. In fact, a thin shell configuration can generate any multipole field of order n with a current distribution $J = J_0 \cos n\vartheta$.

In practice, SCMs are constituted by shells of constant current density, with spacers, in such a way as to mimic the $\cos\vartheta$ distribution, i.e. they are a mix of the two concepts mentioned above. A practical coil cross section can be approximated as sectors of uniform current density shown in Fig. 4. The configuration shown in the figure ($left$) generates an

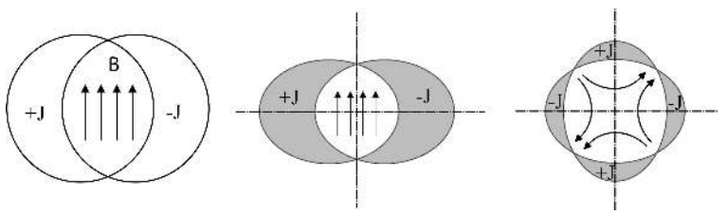

Fig. 3. Uniform dipole and quadrupole fields generated by intersecting circular and elliptical conductors.

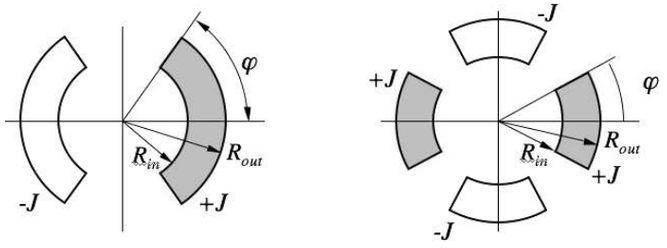

Fig. 4. Principle of sector coils that generate an approximate dipole field (*left*) and quadrupole field (*right*).

approximate dipole B_1, with higher order field errors. Because of symmetry, the only field errors produced (allowed multipoles) are normal multipoles of order $2n+1$, i.e. $B_3, B_5, B_7, \ldots$. Similarly, the configuration in Fig. 4 (*right*) produces an approximate quadrupole B_2 with normal higher order multipoles of order $2(2n+1)$, i.e. $B_6, B_{10}, B_{14}, \ldots$.

In Tables 1 and 2, a set of practical formulae for the main field and errors are reported for dipoles and quadrupoles.

Examining the equations in Table 1 for the field and field errors in the sector coil dipole, we see that a choice of $\varphi = 60°$ cancels the sextupole error B_3. The first nonzero multipole error, the decapole B_5, is a few percent, i.e. much larger (two orders of magnitude) than is acceptable in an accelerator magnet. Better field quality can be obtained by segmenting the sectors using insulating wedges, and using two (or more) nested layers. This adds degrees of freedom that can be used to improve the field homogeneity, at the cost of an increased complexity of the winding. In Fig. 5 we show the coil cross sections of the four large scale superconducting synchrotrons. It is evident how the coils have evolved in complexity to follow the increased demand of field quality. In analogy to the dipole, a choice of a sector angle $\varphi = 30°$ in a quadrupole cancels the first allowed multipole, the dodecapole B_6.

Tables 1 and 2 report other key quantities for the design of an accelerator magnet, namely the resultant forces in a coil quadrant (or octant), the midplane stress and the energy per unit length. An additional quantity of relevance is the coil radial width, $w = R_{\rm out} - R_{\rm in}$, which is used to estimate the overall coil volume, mass and material cost. Tables 1 and 2 can be used to study the functional dependencies of these quantities on the main design inputs, namely the desired field, the magnet aperture and the average current density. As an example,

Table 1. Practical analytical formulae for the dipole field and field errors for the dipole sector coil configuration in Fig. 4 (*left*). The force in a coil refers to a quadrant. The azimuthal stress is intended as average on the coil midplane.

Main field	$B_1 = \frac{2\mu_0}{\pi} J (R_{\rm out} - R_{\rm in}) \sin(\varphi)$
Field errors $n = 3, 5, \ldots, 2i-1$	$B_n = \frac{2\mu_0}{\pi} J \frac{R_{\rm out}^{2-n} - R_{\rm in}^{2-n}}{n(2-n)} \sin(n\varphi)$
	$A_n = 0$
Force per coil quadrant	$F_x = \frac{\sqrt{3}\mu_0 J^2}{\pi} \left[\frac{2\pi - \sqrt{3}}{36} R_{\rm out}^3 + \left(\frac{\sqrt{3}}{12} \ln\left(\frac{R_{\rm out}}{R_{\rm in}} \right) + \frac{4\pi + \sqrt{3}}{36} \right) R_{\rm in}^3 - \frac{\pi}{6} R_{\rm out} R_{\rm in}^2 \right]$
	$F_y = \frac{\sqrt{3}\mu_0 J^2}{\pi} \left[\frac{1}{12} R_{\rm out}^3 + \left(\frac{1}{4} \ln\left(\frac{R_{\rm in}}{R_{\rm out}} \right) - \frac{1}{12} \right) R_{\rm in}^3 \right]$
	$F_z = \frac{3\mu_0 J^2}{\pi} \left[\frac{1}{6} R_{\rm out}^4 - \frac{2}{3} R_{\rm out} R_{\rm in}^3 + \frac{1}{2} R_{\rm in}^4 \right]$
Stress in the mid-plane	$\sigma_\theta = \frac{6\mu_0 J^2}{4\pi} \left[\frac{5}{36} R_{\rm out}^3 + \frac{1}{6} \left(\ln\left(\frac{R_{\rm in}}{R_{\rm out}} \right) + \frac{2}{3} \right) R_{\rm in}^3 - \frac{1}{4} R_{\rm out} R_{\rm in}^2 \right] \frac{1}{R_{\rm out} - R_{\rm in}}$
Energy per unit length	$E/l = \frac{\pi B^2 R_{\rm in}^2}{\mu_0} \left[1 + \frac{2}{3} \frac{R_{\rm out} - R_{\rm in}}{R_{\rm in}} + \frac{1}{6} \left(\frac{R_{\rm out} - R_{\rm in}}{R_{\rm in}} \right)^2 \right]$

Table 2. Practical analytical formulae for the field gradient and field errors for the quadrupole sector coil configuration in Fig. 4 (*right*). The force in a coil refers to an octant. The azimuthal stress is intended as average on the coil midplane.

Main field	$G = B_2 = \frac{2\mu_0}{\pi} J \ln\left(\frac{R_{\rm out}}{R_{\rm in}}\right) \sin(2\varphi)$
Field errors $n = 6, 10, \ldots, 2(2i-1)$	$B_n = \frac{4\mu_0}{\pi} J \frac{R_{\rm out}^{2-n} - R_{\rm in}^{2-n}}{n(2-n)} \sin(n\varphi)$
	$A_n = 0$
Force per coil octant	$F_x = \frac{\sqrt{3}\mu_0 J^2}{6\pi}\left[\frac{1}{72}\frac{12R_{\rm out}^4 - 36R_{\rm in}^4}{R_{\rm out}} + \left(\ln\left(\frac{R_{\rm in}}{R_{\rm out}}\right) + \frac{1}{3}\right) R_{\rm in}^3\right]$
	$F_y = \frac{\sqrt{3}\mu_0 J^2}{\pi}\left[\frac{5-2\sqrt{3}}{36} R_{\rm out}^3 + \frac{1}{12}\frac{R_{\rm in}^4}{R_{\rm out}} + \left(\frac{2-\sqrt{3}}{6}\ln\left(\frac{R_{\rm in}}{R_{\rm out}}\right) + \frac{\sqrt{3}-4}{18}\right) R_{\rm in}^3\right]$
	$F_z = \frac{3\mu_0 J^2}{4\pi}\left[\frac{1}{4} R_{\rm out}^4 - \left(\ln\left(\frac{R_{\rm out}}{R_{\rm in}}\right) + \frac{1}{4}\right) R_{\rm in}^4\right]$
Stress in the mid-plane	$\sigma_\theta = \frac{\sqrt{3}\mu_0 J^2}{\pi}\left[\frac{1}{36}\frac{7R_{\rm out}^4 + 9R_{\rm in}^4}{R_{\rm out}} + \frac{1}{3}\left(\ln\left(\frac{R_{\rm in}}{R_{\rm out}}\right) + \frac{4}{3}\right) R_{\rm in}^3\right] \frac{1}{R_{\rm out} - R_{\rm in}}$
Energy per unit length	$E/l = \frac{\pi G^2 R_{\rm in}^4}{2\mu_0 \left(\ln\left(\frac{R_{\rm in}}{R_{\rm out}}\right)\right)^2}\left[\frac{1}{8}\frac{R_{\rm out}^4 - R_{\rm in}^4}{R_{\rm in}^4} - \frac{1}{2}\ln\left(\frac{R_{\rm in}}{R_{\rm out}}\right)\right]$

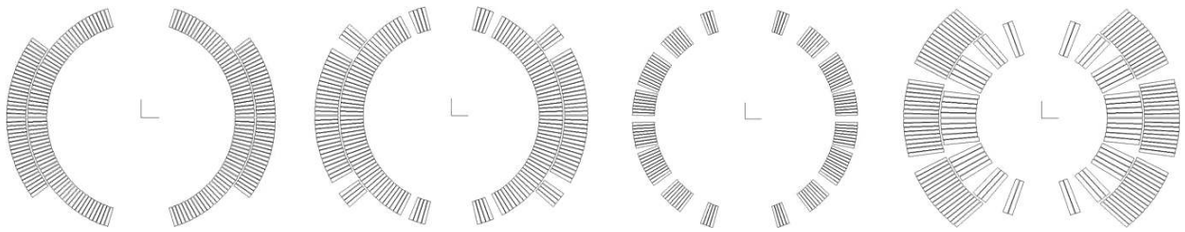

Fig. 5. Coil cross section, to scale, for the dipole magnets of (*left to right*) Tevatron, HERA, RHIC and LHC (for the LHC, only one of the two twin coils is shown).

for a dipole of a given field B and aperture $R_{\rm in}$ we have the approximate relations

$$w \approx \frac{1}{J}, \quad F \approx \text{const}, \quad \sigma \approx J \quad E \approx \frac{1}{J}^{1/2};$$

for a given current density J and aperture $R_{\rm in}$ we have

$$w \approx B, \quad F \approx B^2, \quad \sigma \approx B, \quad E \approx B^{5/2},$$

and for a given field B and current density J we have

$$w \approx \text{const}, \quad F \approx R_{\rm in}, \quad \sigma \approx R_{\rm in}, \quad E \approx R_{\rm in}^{3/2}.$$

Given a design field, the radial width of the coil (and thus the mass and cost of the magnet) scales inversely proportional to the current density in the winding. In addition, at constant coil width, an increase in the current density allows a higher field to be reached. In other words, *the current density is the most important design parameter of accelerator magnets*. In Table 3, the typical overall current density of various systems is reported: accelerator magnets work by far at the highest value, so it is no surprise that they give the strongest reason for the highest current density.

The benefit of superconductivity is evident from the previous consideration. To quantify this benefit, it suffices to note that the LHC ring is 26.7 km and requires some 130 tons of LHe inventory to operate its 8.3 T SCMs. The power at the plug of the refrigeration system is about 45 MW. By contrast, if the LHC had been built with classical resistive magnets at 1.8 T, the circumference would have been more than 100 km long and would have required about 900 MW of installed power (the power output of a large nuclear power plant unit). This would have led to prohibitive construction and operational costs, and in addition it would have had an unacceptable impact on the environment since the 900 MW power is rejected as warm water (at a temperature which is too low for any use).

Table 3. Current density J_{overall} and other characteristics of different types of large magnetic systems.

Magnetic system (only dc)	Current density J_{overall} (A/mm^2)	Operating current (kA)	Typical field range (T)	System stored energy (MJ)
Resistive-air cooled	1–5	1–2	<1	0.01
Resistive-water cooled	10–15	1–10	2	0.05
SC magnets for particle detectors	20–40	2–20	2–6	5–2500
SC Tokamaks for fusion*	25–50	5–70	8–13	5–40,000
SC magnets for MRI	50–200	1	1–10	1–50
SC laboratory solenoids	100–250	0.1–2	5–20	1–20
SC accelerators	200–500	1–12	4–10	1–10,000

*Top figures refer to ITER, under construction.

We also note from the above scaling that the forces in a dipole scale proportionally to the magnet aperture, and with the square of the field. The accuracy of the scaling is demonstrated in Fig. 6, where we report the horizontal and vertical forces in the coil quadrant of the dipoles of the four large scale superconducting synchrotrons, and the SSC. The scaling is reasonably accurate, better than 20%, for magnets that cover a relatively large span of the field and aperture.

The large increase in force makes it clear why the mechanical design of high field magnets is challenging, and why in general high field magnets tend to have the minimum practical aperture. We see, however, that if the coil is designed for a given current density, which is usually the case, the stress in the coil increases only linearly with the field. This is because the width of a coil with given current density also increases linearly with the bore field, thus providing more material to resist the force. In fact, the stress can be lowered by reducing the current density in the coil and/or R_{in}, as indicated by the scaling relations above.

A final interesting result of the scaling analysis is that the magnet energy per unit length is also a strong function of the bore field and aperture. As in Fig. 6, we have reported in Fig. 7 a summary of the energy per unit length in the dipoles of the four large synchrotrons, and the SSC. Here, again, we see that the scaling works fairly well. The difficulty associated with the increase in stored energy is the protection of the magnet (and the chain of magnets, in particular) in case of quench, to be discussed later.

2.2.2. *Alternative configurations*

Alternative coil shapes have been considered in the design of SCMs. An interesting alternative to $\cos\vartheta$ is the use of coil blocks rectangular in shape. However, in addition to the lower coil efficiency

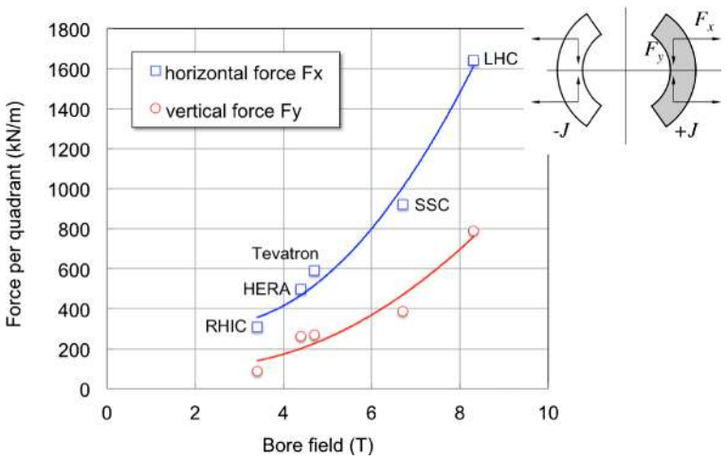

Fig. 6. Horizontal and vertical force on one coil quadrant (see inset), computed for the superconducting dipoles of the main high-energy colliders, and the SSC, and plotted vs. the dipole field in the magnet bore.

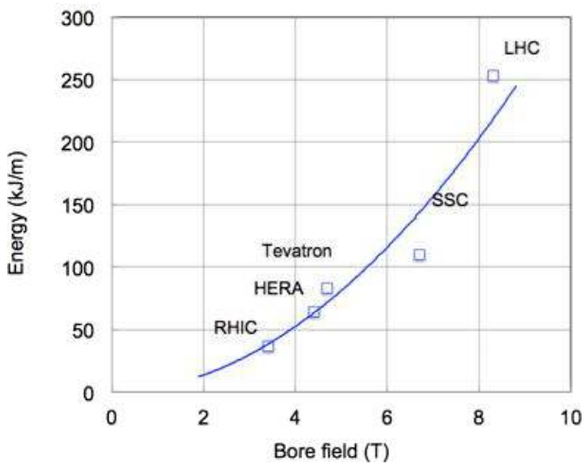

Fig. 7. Stored energy per unit length per aperture, computed for the superconducting dipoles of the main high-energy colliders, and the SSC, and plotted vs. the dipole field in the magnet bore. For LHC the energy is for one bore only.

(more conductor for the same central field and field quality), past experience is that block coils have had lower performance. This suggests that the spectrum of mechanical perturbations may have a larger amplitude for this type of coil shapes. A block coil configuration is suitable for low field magnets, when the iron field is predominant, like for FAIR-SIS100 [5]; see Fig. 8.

The configuration of canted or tilted coils, proposed for the SSC, has recently been developed again [6]. It looks like a "canted solenoid," where two layers are wound in such a way that the azimuthal components of the current of two adjacent layers cancel out, so that only the longitudinal one, the one generating a transverse field, remains; see Fig. 9. Its advantage is the use of single wire or small cables and apparently is very easy to wind with small tooling, like a solenoid. While it is very appealing for certain applications, like small and slim coils that have to be bent to follow a beam trajectory, its advantage for fairly good size coils is not very clear since the effect of the azimuthal current is canceled out but the conductor is still there. In addition, it seems difficult to use with large cables, and so the inductance is most probably very high (see the discussion on protection).

A general study of coil configurations and their merits has been carried out in Refs. 7–9.

2.2.3. *High current density*

As mentioned above, the current density in the whole coil block is the first and key parameter. When referring to the overall cross section of the coil, we will use $J_{\text{overall}} \equiv N_{\text{turn}} \cdot I/A_{\text{coil}}$, where I is the current in a turn, N_{turn} the total turn number in the coil and A_{coil} its cross section. It is also useful to define two other current densities: (i) the critical current densities, $J_c \equiv I_c/A_{\text{sc}}$, where A_{sc} is the cross section of the superconducting (noncopper) material in the conductor and I_c is the critical current of the conductor, i.e. of the turn; (ii) the critical engineering current density, $J_e \equiv I_c/A_{\text{cond}}$, where A_{cond} is the total cross section of the conductor where the current can

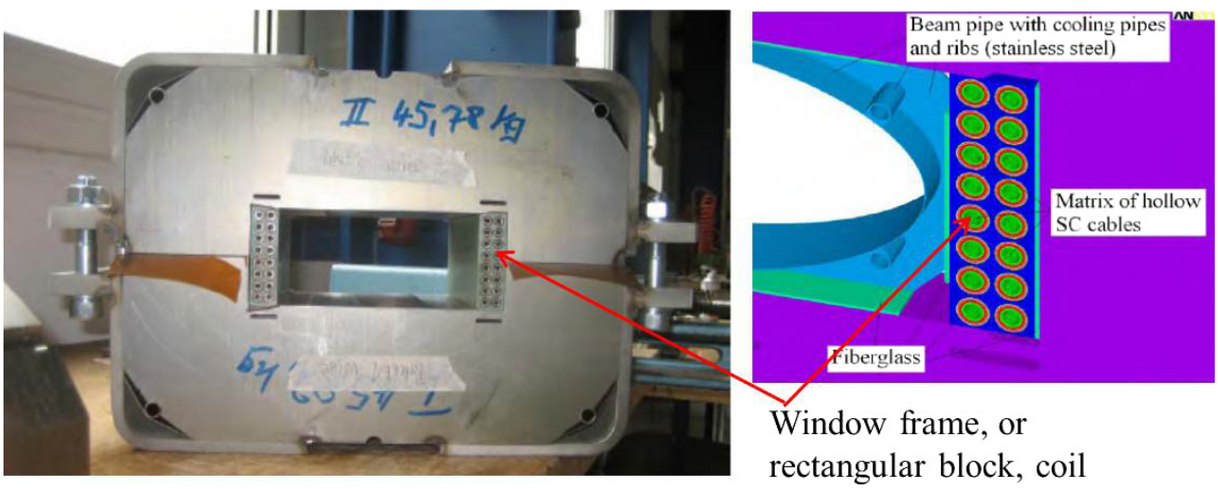

Fig. 8. Picture and schematic of the early cross section of the FAIR-SIS100 dipole (courtesy of E. Fisher, P. Schnizer, GSI).

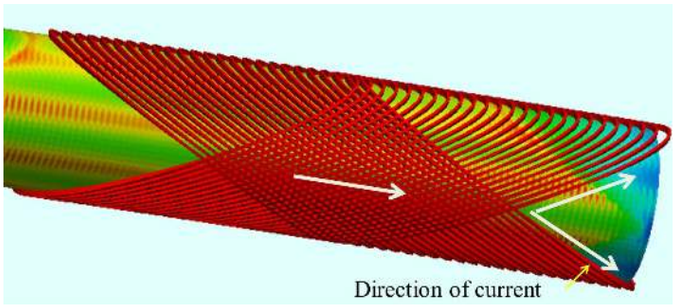

Fig. 9. Schematic of the canted solenoid coils for generating a pure dipole field (courtesy of S. Caspi, LBNL).

flow. In practice $A_{\text{cond}} = A_{\text{sc}} + A_{\text{stab}}, A_{\text{stab}}$ being the cross section of the part that is added to the superconductor for stabilization purposes (see the next section). J_c is a property of the material, i.e. of the type of superconductor and of the metallurgical manufacturing process, while J_e takes into account that the practical conductor needs stabilizer, barriers, substrates or stress retainer. J_e is an important parameter also for stability and protection (to be discussed later). Let us now discuss the role and interplay of these parameters.

- *High J_c.* This is the basic parameter and it is of course of primary importance. We need to operate the system at a value not far from the critical current; therefore, J_c must be not only high but also very uniform. For example, the LHC dipoles work at 86% of the crossing of the load line with the critical current curve, and they have been designed and tested to 93% of it: a 5–10% variation in the J_c performance, usually negligible in other systems, directly impacts on the accelerator magnet's performance.
- *Low stabilizer content.* High purity copper is of course necessary but we need to keep it to a minimum compatible with the stabilization and protection requirement, to avoid excessive lowering of J_e. Usually Cu/SC (or Cu/non-Cu) ranges between 1.5 and 2 for Nb–Ti-based systems and 0.9 and 1.5 for Nb_3Sn magnets, just the minimum for stabilization and dangerously near to the minimum for protection: we need to protect magnets with such low copper content although the stored energy can be as high as 7 MJ for LHC magnets.
- *High compaction cable.* Use of flat double face cable, with transposed strands, called Rutherford cable, is the invariable choice. The reason for the success of Rutherford cable is mainly its 90% compaction factor (which increases to 93–94% after coil curing). The interstice between strands is such as to allow helium to percolate inside to increase stability, for Nb–Ti magnets. Such high compaction is not trivial, considering the difficulty of manufacturing large, multi-kA cable, but is beneficial for maintaining a high J_{overall}.
- *Thin insulation.* Total interturn thickness is less than 250 μm for modern accelerator magnets, usually in polyimmide tapes, in the presence of a kV range discharge voltage and GJ stored energy in the circuit. Again, the use of thin insulation is mandatory in order to keep J_{overall} high.

Engineering and optimization of the above parameters, illustrated by the practical example of the LHC dipole coil package in Fig. 10, allows the building of systems with stored energy in the range of 0.1–1 GJ, with an overall current density, J_{overall}, at the level of 400 A/mm^2. To provide a meaningful benchmark, systems with similar energy are usually built with much less compacted cables, or a much higher amount of stabilizer, and insulation thickness in the range of 1 mm, which finally yields J_{overall} ten times smaller; see Table 3.

2.2.4. *Superconductor, load line and margins*

Superconducting materials and cables are discussed elsewhere in this volume [10]. It is worthwhile here to report on the practical materials that can be used for magnets, making reference to Fig. 11, where J_e is plotted versus the field for the few practical materials, out of the many tens of thousands of known superconductors. In practices all present accelerators have used Nb–Ti; Nb_3Sn, which can open the way to a field above 8–9 T, is on the verge of being

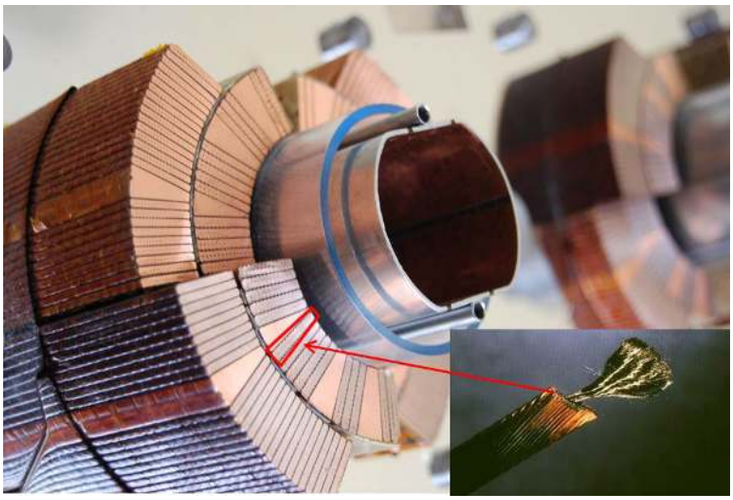

Fig. 10. Picture of the LHC dipole cross section showing details of the coil around one of the two beam pipes (see drawing in Fig. 3 and Fig. 5 for a better understanding). The highly packed coil demonstrates the concepts discussed in the text. An LHC cable with partially etched strand is shown in the inset.

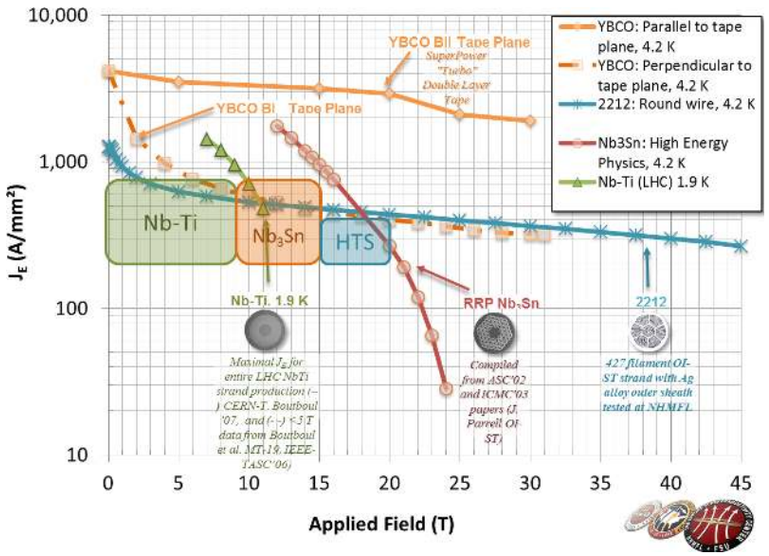

Fig. 11. Engineering current density of high field superconductors (courtesy of P. Lee, Applied Superconductivity Center of FSU, Florida).

fully mature for accelerators; see Sec. 6. MgB_2 is a niche material: bound to the 4–15 K temperature range and good only for relatively low fields, 1–5 T, it may in the future compete with Nb–Ti since potentially it has a very low cost. However, the current performance is still short of that for standard Nb–Ti, while the mechanical properties, quality (filament diameter) and uniformity are much worse. The only advantage is its critical temperature, which entails a large stability margin: for this reason it may be useful for fast synchrotron magnets, where steady heat release is an issue.

HTSs (high temperature superconductors), with which we indicate Bi-2212 or YBCO, are interesting only for fields above 15–16 T, a range that is hardly achievable by Nb_3Sn for accelerators, even at 1.9 K. To date, only preliminary R&D studies using these materials for this type of magnets are underway.

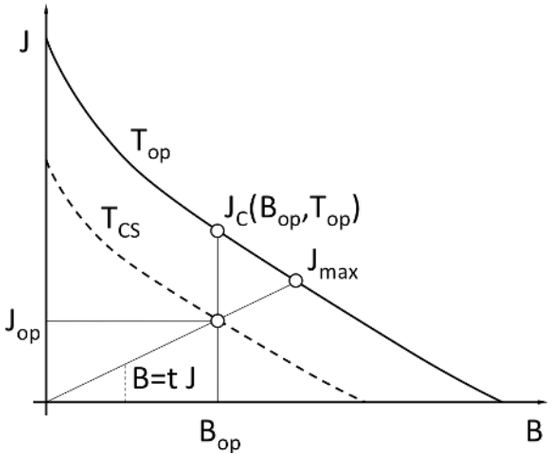

Fig. 12. Magnet design chart: critical current curves of a superconductor versus the field at the operating temperature and at transition (current sharing between SC and stabilizer).

Despite all the effort to work at the highest current density, the operating point of a SCM must be chosen to be well below the critical current of the material (see Fig. 12), i.e. with proper *margins* that ensure *stability* at the operating point. The typical metrics used for operating margins are:

- The critical current margin i, the operating fraction of the critical current density $i = J_{\rm op}/J_c(B_{\rm op}, T_{\rm op})$;
- The margin along the load line l, the ratio of operating to critical current, $l = J_{\rm op}/J_{\rm max}$, where $J_{\rm max}$ is the critical current evaluated at the intersection of the magnet load line and the critical surface (see Fig. 12): $J_{\rm max} \equiv J_c(tJ_{\rm max}, T_{\rm op})$;
- The temperature margin ΔT, the difference in temperature from operating conditions $T_{\rm op}$ to current sharing conditions $T_{\rm CS}$, evaluated at the operating field and current density, $\Delta T = T_{\rm CS}(J_{\rm op}, B_{\rm op}) - T_{\rm op}$. The current sharing temperature is the temperature at which the operating current density equals the critical current, or $J_{\rm op} = J_{\rm C}(B_{\rm op}, T_{\rm CS})$.

Representative values for the design of the large scale accelerator dipoles listed earlier are $i \approx 0.5, l \approx 0.8$ and $\Delta T = 0.5, \ldots, 1.5\,{\rm K}$.

An additional quantity that measures the stability of the operating point is the energy margin, i.e. the quantity of heat necessary for driving the superconductor normal. The energy margin is actually the primary indicator of the stability margin, but it depends on the time and space characteristics of the heat deposition, as discussed in the classic textbook by M. N. Wilson [11]. A lower bound of the energy margin is given by the enthalpy difference between operating and current sharing conditions, $\Delta H = H(T_{\rm CS}) - H(T_{\rm op})$. A robust magnet design is such that the energy margin is larger than the expected amplitude of perturbation over the whole spectrum of operating conditions and characteristic times.

The margins defined above are shown graphically in Fig. 12, which can be seen as the main design graph for an SCM. A schematic critical current density is plotted together with the magnet load line (field versus current density) of the peak field $B_{\rm peak}$, i.e. the point where the field is highest among all volumes of the superconductor. The intersection of the load line of the peak field with the critical current curve of the superconductor itself determines the theoretical maximum performance of the magnet. This value is often called — with bad jargon! — the short sample limit, since the critical current is that of a "short sample" cut out from the unit length of the conductor, assumed to be representative of the intrinsic performance of the superconductor used to wind the coil. We will call that maximum value the *magnet critical field*, or *magnet maximum current*,[a] $I_{\rm max}$. The central field B_0 corresponding to the magnet critical current is lower than the peak field. The ratio $\lambda \equiv B_{\rm peak}/B_0$ can be used as a measure of the efficiency of a coil design: indeed, $B_{\rm peak}$ is at the maximum equal to $B_c(T, I)$, which is a superconductor property. Therefore λ limits the performance of the "useful" field B_0. In superconductivity there is a strong penalty for a configuration using too much conductor, not only because superconductor is expensive, but because it inevitably means less performance, owing to λ being larger than 1. For transverse uniform fields, only an ideal $\cos\vartheta$ configuration yields $\lambda = 1$. A good design can achieves $\lambda = 1.1$ or lower, which is quite an acceptable figure.

[a]The actual maximum current of a magnet may be lower, for other design limitations — forces, cooling, etc. — or just for lack of performance. With $I_{\rm max}$ here we indicate the maximum "intrinsic" current as given by superconductor properties and e.m. design.

2.2.5. *The iron yoke*

The coils are usually inserted into an iron yoke; see Fig. 2. When the iron is not saturated, it can be approximated analytically using the method of images, which is simple in the case of a round iron cavity. A compact treatment of this method can be found in Ref. 12. For complex geometries, or in the presence of saturation, it is mandatory to resort to computer codes to perform the appropriate calculations and optimizations. The yoke contribution to the field may seem relevant, typically 10–20%, even for conductor-dominated magnets. Actually it can be partly offset by an increase in the current: without iron the field on the coil decreases much more than the central field, giving an extra margin on the load line. So its main function is to lower the current density for a given field, which is very beneficial for protection and integration. Of course, the yoke's basic function — to provide a flux return path, avoiding an excessive stray field — remains essential.

2.2.6. *Field quality and harmonic content*

An almost unique characteristic of accelerator magnets is the necessity of a very high field quality. By using the multipole expansion Eq. (2), which provides the harmonics of the series in the complex plane, the field content of each pole can be evaluated in relative terms to the main field $b_n = 10^4 B_n/B_{\text{main}}$. The factor 10^4 is used to scale the relative harmonics to practical *units*. As an example, 1 unit of b_3 content in a dipole means that the sextupole field is 0.01% of the dipole field. We can see readily from Eq. (2) that the dipole component is constant over the magnet aperture, while the field of each component grows with the radius R as $B_n \propto R^{n-1}$. The units of the harmonic content, measured at the radius given by the measuring system, are scaled to a reference radius which is relevant for the specification of the field quality. Customarily, the reference radius is taken as two-thirds of the magnet radius because this is the portion of the aperture allocated to the beam trajectories, the rest being necessary for the beam pipe, insulation, etc. By using this criterion, i.e. the field quality at two-thirds of the coil aperture, it is possible to compare field quality among magnets of different apertures.

When considering the absolute demands on field quality, we note that field accuracy at the 10–100 ppm level is not extraordinary. Indeed, in other types of superconducting systems, and especially for MRI and NMR magnets, homogeneities at the ppm level are not uncommon. What is extraordinary in accelerator magnets, and in particular for colliders, is that such accuracy of 10 ppm is required at a distance of 10 mm or less from the conductor (in an MRI magnet the ppm accuracy is required at a more than 100 mm distance from the main coils).

At such a small distance, the small cable deformations affect the harmonic content, and the superconductor magnetization has quite a visible effect on the field quality.

A superconducting cable reacts as a diamagnetic material to a change in the external field: shielding currents are induced in the superconducting filaments, also referred to as *persistent currents*, and among filaments in a strand or among strands in a cable, also referred to as *coupling currents*. Persistent currents have an ideally infinite time constant of decay; they depend linearly on the value of the critical current density (which cannot be reduced!), and on the size of the superconducting filaments, which is therefore made as small as is practical. Examples of the contribution of the persistent current magnetization in the LHC's main dipole magnets are shown in Fig. 13. We report the measured average and spread of the main field b_1 and the sextupole b_3 over all the magnets tested in cryogenic conditions. It is instructive to compare the magnitude of the effects measured and reported in Fig. 13 to the field quality specifications derived from stability and control criteria on the LHC beam. These targets are 1 unit of reproducibility from one physics run to the following one for the dipole transfer function (to achieve rf capture of the injected beam), and 0.02 units of the sextupole b_3 (to control the chromaticity). They are much smaller than the measured magnitude of the effects, which therefore must be made reproducible in order to be corrected very accurately.

Coupling currents in strands and cables flow in loops formed among the superconducting filaments, with a return path across the wire matrix, or the strand contacts [10, 13]. The amount of coupling depends on the geometry of the current loop, which is made as small as possible by twisting, and on the resistivity of the matrix or the strand contacts. The amplitude of the coupling currents is proportional to the field change rate. Resistance control measures,

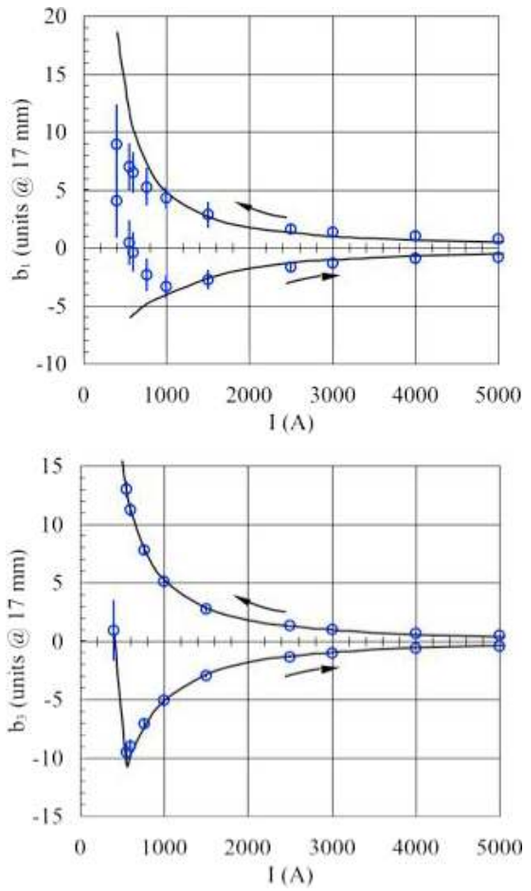

Fig. 13. Variation of main field (b_1) and sextupole (b_3) components, generated by superconductor magnetization, in an LHC cycle.

such as resistive barriers in the strand matrix, resistive coating to the strands, or inserting resistive barriers (sheets, wraps) in the cable, are used effectively to limit the amplitude of coupling currents. Indeed, coupling currents have always been well controlled for any of the large scale synchrotrons mentioned earlier. This may change in fast-cycled synchrotrons (see Sec. 5), and for high field magnets (see Sec. 6).

Materials such as Nb_3Sn, with large current density and filaments, or HTS cables built with tapes will introduce a new challenge in the control of magnetization effects. Nb_3Sn of HEP grade has very large magnetization, one order of magnitude larger than the Nb–Ti used so far, thus giving much larger effects. In addition, it is plagued by flux jumps which result in fast variations of the field, and have no reproducible behavior.

A final word about accuracy: the main magnets, i.e. the ones composing the optical lattice, are powered in series. Proper control of the beam parameters requires that the integral field per unit current of each magnet, usually called the "transfer function" (for a dipole: the bending strength per unit current in Tm/A), be equal to within 10^{-4}–10^{-3}. For a series production like the LHC, this was one of the toughest requirements which was eventually met. For comparison, magnets for other uses, like spectrometers, detector magnets, fusions, and even NMR or MRI, require a relatively modest precision of 0.5–1%. In the case of superconducting cavities for accelerators, even differences in the range of 1–10% in performance are acceptable.

2.3. *Magnet structure and forces*

Restraining the e.m. forces with the magnitudes mentioned earlier is a big endeavor in transverse fields. As can be seen in Fig. 1, the radial force support must all come from external structure, since in this direction there is not any coil self-support (like it is for solenoids and partially for toroids), while the longitudinal forces near the coil ends are partially self-supported by the coil. The other big problem is the presence of strong azimuthal forces, compressing the coils toward the midplane. This is of course the same effect that we have in solenoids; however, here we want to avoid movement at any cost because the interference of coils with support structure and between layers will generate friction and the stick-and-slip regime [14]. Therefore we need to give a fair amount of azimuthal prestress to avoid conductor motion during magnet excitation. The best way for $\cos\vartheta$ configuration is to use the *Roman arch* structure, giving precompression by carefully inserting an oversized wedge into the pole region. Coupling the Roman arch concept with a circular band to give the radial prestress generated the collar concept, developed first at Fermilab [15] and illustrated in Fig. 14 for the LHC twin dipoles. Collars are locked by means of very precise external keys (for single bore coils) or by pinning rods (LHC) and provide in an effective way azimuthal and radial prestress.

The coil–collar pack is then inserted into the iron yoke. The yoke can be outside the coil cryostat, at room temperature, as it is for the Tevatron magnets, or it can be part of the cold mass, inside the cryostat, as implemented by HERA [16]; see Fig. 15.

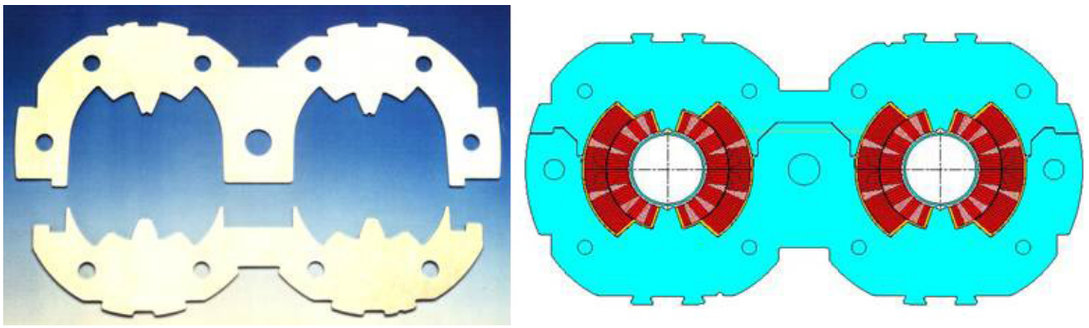

Fig. 14. Collar pair of an LHC dipole before (*left*) and after (*right*) being locked onto the coils.

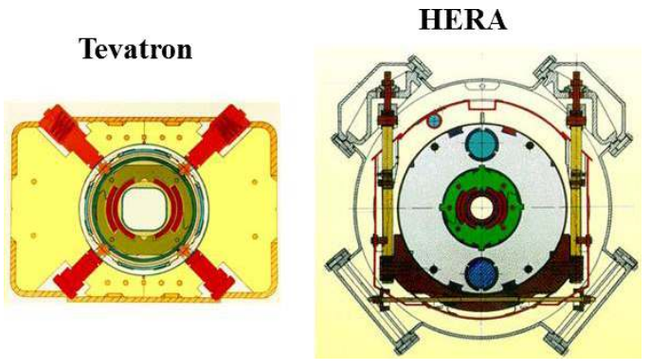

Fig. 15. Cross section of the warm iron Tevatron dipole and of the HERA dipole.

The coil–collar pack can be free-standing inside the iron yoke, with only pins to provide alignment.Up to 5–7 T collars can be made strong enough to support alone all the e.m. forces.

However, in dipoles at higher fields the collars need to be assisted by additional compression given by an external cylinder via the iron yoke. The compression of the external cylinder can be attained by welding-generated prestress and/or by differential thermal contraction. Compression by the external cylinder via the iron yoke requires a careful line-to-line fit of the collar–yoke interface and precise control of the thermal stresses due to cool-down. External prestress must always be carefully balanced, between radial and azimuthal, to avoid bending moments which can create high peak stress.

Other schemes for prestressing are possible: the most successful is the one used for RHIC magnets [17]: the coil is surrounded by thin collars with no support function; they are just spacers between coil and iron and serve for assembling and handling. The yoke is assembled onto the coil pack and prestressed by keys and enclosed by an external shrinking cylinder, again via welding or thermal contraction.

A novel concept, based on a bladder and shells, has recently been devised to lock the coils without collars; it will be discussed in Sec. 6, which is devoted to future magnets.

2.4. *Quench detection and protection*

SCMs, like any superconducting device, require a fail-safe quench detection and protection system to insure that a resistive transition does not cause a thermal runaway and damage. In short, the main issues for HEP magnets are the large current density in the conductor, and the large magnetic energy stored per unit coil mass. To fix orders of magnitude, during a resistive transition at nominal operating current in an LHC dipole, the current density in the copper stabilizer is approximately $700\,\mathrm{A/mm^2}$. This corresponds to a Joule power density of $70\,\mathrm{MW/m^3}$ at 20 K, increasing by more than two orders of

magnitude at room temperature. Such a power density, if the current stayed constant through the resistive transition, would be enough to bring copper to melting temperature in approximately 0.3 s. It is obviously mandatory to switch off the power supply, typically on a timescale 10 times faster than above, as soon as a quench is detected by using balanced bridge measurements. This is, however, not enough, because the magnet, an inductance L, stores a large quantity of energy E that drives the current during the dump process. The purpose of a sound design of a well-protected magnet is to make sure that nowhere in the coil do the temperature, thermal stresses and voltage exceed allowable values. The peak temperature $T_{\rm hot}$ reached during a quench (also called the *hot spot*) is one of the fundamental indicators. Accelerator magnets, with well-controlled and highly loaded mechanical structures, can tolerate temperature increases up to room temperature conditions, — 300 K. The hot spot temperature can be estimated using an adiabatic heat balance, equating the Joule heat produced during the discharge to the change of enthalpy of the conductor

$$\int_{T_{\rm op}}^{T_{\rm hot}} \frac{C}{\rho} dT = \frac{1}{A_{\rm cu} A_{\rm tot}} \int_0^\infty I_{\rm op}^2 dt, \qquad (3)$$

where C is the total volumetric heat capacity of the superconductor composite, and ρ is the resistivity in the normal-conducting state. We see from the above concept, borrowed from electrical blow fuse design (whence the improper analysis in terms of *MIIts*), that to limit $T_{\rm hot}$ for a given value of the integral on the right hand side of Eq. (3), it is always advantageous to reduce the normal state resistance and the time of the discharge. The normal state resistance is decreased by backing the superconductor with a matrix of a stabilizer material with good conductivity properties (e.g. copper) and increasing the percentage of stabilizer in the composite. The speed at which the energy dump takes place, on the other hand, depends on the magnet inductance and the resistance of the circuit formed by the quenching magnet and the external circuit formed by the power supply, switch and dump resistor, or $R = R_{\rm quench} + R_{\rm ext}$. The characteristic time of the dump is then $\tau \approx L/R$, which can be made short by decreasing the magnet inductance and/or increasing the resistance. For a given magnet geometry and stored energy, the magnet inductance is inversely proportional to the square of the conductor current, which is the motivation for the use of large current cables. As to the resistance, practical considerations limit the terminal voltage to the range of 1 kV or less, which gives an upper limit to the external resistance of the magnet that, in the most optimistic case, is only marginal for the protection of a single magnet. Since the growth of the natural quench resistance may also be too slow, especially in the presence of a matrix with low resistivity required to enhance stability and beneficial to keep the left hand side integral of Eq. (3) small, protection ultimately relies on active quench initiation, triggered by heaters embedded in the winding pack, and fired at the moment a quench is detected to spread the normal zone over the whole magnet mass.

In certain cases, the current decay is so fast that eddy currents induced in the metallic part of the coil package may generate as much heat as to quench part of the coils in the first part of the decay. This phenomenon, called "quench-back," is usually beneficial in reducing $T_{\rm hot}$. Active quench initiation has the additional benefit of making the temperature and voltage distribution more balanced, reducing thermal and electrical stress.

As mentioned earlier, in synchrotrons and colliders the magnets are powered in series. Therefore the stored energy in a single circuit is much larger than the energy stored in a single magnet, e.g. of the order of tens of MJ, up to the 1 GJ stored in each of the eight circuits formed by the series of 154 LHC main dipoles. This configuration is such that the discharge time, under reasonable terminal voltage, would be orders of magnitude longer than required for the protection of a single magnet. As an example, an external dump resistor would require a voltage of hundreds of kV. Protection in this case relies on the expedient of subdivision of the circuit, so that each magnet can be discharged independently. Each magnet is bypassed by an SC line (bus bar) with a diode that opens only in case there is voltage across the magnet. The quench induced by the heaters insures that the quench voltage is sufficient to open the diodes. The current through the quenched magnet decreases while its magnetic energy is dissipated in the quench resistance, and the diode carries the current of the whole line, which is dumped with a much longer time constant. The above concepts and solutions, whose description has been inspired by

the LHC layout, are applied in similar fashions in all large scale HEP machines, as well as other SCM systems. Indeed, many other SC systems are protected by diodes; however, none of them have diodes with a capacity of 13 kA at 1.9 K.

2.5. *Integration*

A superconducting accelerator depends on single magnets, as described so far, but, as the reader may have suspected, it also possesses a system dimension whose final performance depends on the successful integration of all single elements. In a classical alternating gradient configuration, dipoles and focusing/defocusing quadrupoles are alternating in well-defined periods (cells). The sequence of main magnets is complemented by regularly spaced orbit correctors, trim and correction quadrupoles, sextupoles and higher order corrector magnets, all acting either as a normal or a skew component. Most of these magnets are powered in families that must be connected in series. A large number of bus lines carrying the current of each magnet type need to run along the whole circuit, and specifically across magnets of other types. As an example, in the LHC dipoles and quadrupoles the cold mass needs to lodge three pairs of high current bus bars (one dipole circuit and two quadrupole circuits) for the main quads and some 30 pairs of smaller current SC bypass buses, with problems of space, voltage insulation, e.m. cross-talk, etc. All these lines need to be electrically connected, usually with soft soldering, at each magnet extremity. This region, the *magnet interconnect*, in addition to lodging the electrical connections, provides hydraulic continuity to the various coolant feed and return lines, vacuum tightness for the primary (beam) and secondary (insulation) evacuated spaces, electrical continuity of the low impedance liner surrounding the beam space (the beam screen in the LHC), and must cope with the differential contractions and forces that arise during cool-down, warm-up and cryogenic operation. All these issues, and many others, like the necessity of precise alignment, are usually considered much less technically complicated than the SCM proper. Nonetheless, they increase the system complexity, with many interfaces that need to be properly managed. We will return later to this topic, while describing the September 2008 LHC incident.

3. Brief History of Superconducting Magnets for Accelerators

3.1. *Early history*

Intensive R&D programs were launched in many laboratories to develop superconducting accelerator magnets as early as the late 1960s. This article is necessarily a partial recollection of the main steps and achievements of the past 50 years, where, for the sake of simplicity and compactness, we do not mention many valuable projects and studies: a valuable review of the SCMs from the Tevatron to the LHC can be found in Ref. 18.

The beginning of the history of SCM technology for accelerators can be placed at the start of the 1970s, when more or less at the same time Martin Wilson at RAL (UK) and Bill Sampson at BNL were able to produce the first SC dipole and quadrupole. The EU effort was federated in a collaboration (GESSS) aimed at producing a prototype for the 300 GeV proton synchrotron, the new CERN flagship project called SPS. With a 7-km-long ring, a 4.5 T superconducting SPS would have reached 1 TeV beam [19]. However, ramped magnets (with a field sweep of nearly 1 T/s), as needed for synchrotrons, were still too difficult for the early infancy stage of SCM technology. CERN went on with the resistive magnet project and SPS finally was commissioned at 400 GeV in 1976. The advantages of SCMs, and particularly quadrupoles, were readily recognized. CERN engaged in a project to increase the luminosity of the ISR proton–proton collider (the grandfather of the LHC) by means of powerful large aperture superconducting quadrupoles rated for 5 T [20]. Indeed, by 1980 the eight 1-m-long SC low-β quadrupoles of the ISR were the first SC magnets operated on an accelerator. However, with the construction of the "conventional" SPS, the spotlight definitively migrated to the USA for the following decennium.

3.2. *Tevatron and Isabelle*

In the USA, two projects fought the good battle at the turn of the 1970s. The recently established Fermilab, under the vigorous leadership of the legendary R. R. Wilson, was pursuing a project to go beyond its own record of 500 GeV proton energy of the Main Ring (inaugurated in 1976, just one month before the CERN SPS). Less conservative

than CERN management, Wilson believed in superconductivity and launched what became, through the name of Energy Doubler and then Energy Saver, the Tevatron [21], a collider where magnets, after a very slow synchrotron mode at less than 100 mT/s, stay at the flat top for hours, the ideal mode for superconductivity. The name was obviously chosen to mark the new level of record energy granted by using the new superconducting technology. One brilliant idea of Fermilab scientists was to accelerate the proton–antiproton in the same magnet ring (and one beam pipe), saving a second ring: this required a magnet aperture of 75 mm.

Even before Fermilab, BNL had engaged in long and fruitful R&D [22], eventually converging to the design of 4 T magnets for Isabelle, later renamed CBA (Colliding Beam Accelerators), a 200 + 200 p–p collider. After a very promising initial success, magnet development for a "better" 400 + 400 GeV accelerator based on 5 T field dipoles took longer than expected, resulting in delays. The good progress of the construction of what was to become the Tevatron at Fermilab, and the discovery by CERN's Carlo Rubbia in 1982 of the W and Z bosons, took much wind from the sails of Isabelle, by then appearing redundant. In July 1983, while the SC Energy Saver at Fermilab produced the first beam at 512 GeV, Isabelle was stopped in favor of a much higher energy collider, the SSC (see later).

The success of the Tevatron marked the rise of superconductivity for accelerators: with 7 km at 4.2 K and more than 700 6-m-long SCMs working in series, it really demonstrated the viability of superconducting accelerator magnet technology. The success of Tevatron magnets was based on two technically decisive advances: the first one was the use of the Rutherford cable, with a compaction factor of 90%, some 20–30% more than the braided cable used by the Isabelle magnets; the second one was the development of the collar system for prestress; see Subsec. 2.3. A big difference was that the Tevatron went on with the design of a warm yoke, while Isabelle dipoles had the iron yoke included in the cold mass. This second solution avoids many problems of coil centering and alignment. However, it makes the cool-down and warm-up cycle very long, something that was feared by Tevatron designers in view of possible frequent stops for maintenance/repair (in a proton collider the availability of the machine is almost as important as the peak performance). However, all subsequent projects followed the solution of cold iron, as for the BNL design.

3.3. *HERA and UNK*

In the 1980s, the DESY laboratory in Hamburg started construction of HERA, an e–p collider whose proton ring was based on SC dipoles of 4.7 T at 4.6 K, later operated at 5.5 T by subcooling below 4 K. Very similar in field and aperture to the Tevatron, as well as in quantity (the HERA proton ring was of similar size), the approximately 500 9-m-long HERA dipole magnets [17] marked a few innovations with respect to the Tevatron: (i) use of cold iron, as mentioned in Subsec. 2.3, with an external steel cylinder acting only as a He vessel; (ii) use of free-standing aluminum collars, i.e. the thermal contraction was a critical factor in the coil prestress; (iii) it was all manufactured in industry, while all the pioneering Tevatron magnets were laboratory-built. HERA was very successful in all respects; only the use of a relatively large filament diameter in the Nb–Ti cable (15–17 μm, against the 10 μm of the Tevatron) posed an unnecessary operational challenge that had to be met.

Meanwhile, the Institute of High Energy Physics (IHEP) in Protvino, Russia, was striving to build a 3 TeV, 21-km-long, single ring synchrotron for fixed target experiments (to be eventually complemented in a second phase by a second ring to work in collider mode). Based on 2100 6-m-long, 5 T dipoles, rated for about 100–300 mT/s at 4.4 K, UNK dipoles had a very good design and a comfortable margin (they reached more than 6 T) [23]. However, in 1994 the SC ring project was practically stopped because of the political and economic crises in the former Soviet Union.

3.4. *RHIC*

The Relativistic Hadron Collider was built in the 1990s in the tunnel prepared for the dismissed Isabelle. The ion beams in the two intersecting independent rings, 3.8 km long, are guided by dipole magnets of 3.5 T field [17]. Here the challenge was not the field level, but the low cost. Built in parallel with its giant brother, the SSC (see the next section), it had a limited budget, diminished over many years.

The main new features introduced by the RHIC magnets were: (i) use of iron lamination, locked by keys and restrained by an external cylinder through weld-shrinking, to precompress the coils surrounded by inexpensive thin plastic collars which served as coil positioner only; (ii) careful design of the magnetic field in the presence of a very important contribution of the iron yoke with strong nonlinear effects; (iii) use of magnetic measurements during production, both as a quality tool and to allow "on-line" correcting actions, mostly but not only with magnetic shimming. Not least, the superconducting cable was of very high quality (an important spinoff from the R&D for the SSC) with high J_c fine filaments, and control of J_c and copper content thanks to the world class superconductor test facility of BNL.

3.5. *LHC and SSC*

3.5.1. *The rise and fall of the giant: SSC*

The Super Superconducting Collider (SSC) has been a leading project for accelerator SCM development, backed by a joint effort of all major US laboratories. From the 1983 to 1993, the year of its halt and cancelation by the US Congress, the R&D for the 87-km-long proton–proton collider marked the magnet progress. An optimization study fixed the operating field of the 15-m-long single bore dipole to 6.6 T, the maximum for a 4.4 K temperature operation, in order to meet the target of 20 TeV per proton beam. The design was based on austenitic steel free-standing collars and cold iron with no mechanical function. The collar technology was improved to reduce the spring-back effect during assembly by using tapered keys, which are inserted by means of hydraulic pistons in a state very near to their final load [24]. This is particularly important in order to limit the loss of prestress and avoid excessive mechanical loading of the SC coils during the collaring process. Among the breakthroughs made in the frame of the SSC R&D, one has to mention the increase in J_c from 2000 to >2700 A/mm^2, 5 T–4.2 K, in conjunction with high quality fine filaments of 5–6 μm and the new cable insulation based on full polyimide. However, a number of technical choices were probably not fully optimized — contributing, with bad management and adverse circumstances, to the decision to cancel the project. Among them one has to mention the use of single bore magnets which required two complete separate rings: the highly criticized LHC twin dipole LHC design proved to be right, and 15% less expensive. The working point was very ambitiously near to the critical surface (only a 0.6 K temperature margin), because of the desire to approach a high field without taking up the possibility offered by superfluid helium — considered too complex. Stability, training and other effects made the R&D long [25] and expensive; the increase of the bore from 40 mm to 50 mm, without reducing the field, made performance more difficult to attain, which contributed to the cost escalation that eventually led to the Congress decision to cancel the project.

3.5.2. *LHC: "small and smart"*

The LHC was starting R&D at the end of the 1980s, with very low profile and funding. It relied a lot on the SCC R&D. However, to take full advantage of the existing 26.7-km-long LEP tunnel, it pushed the Nb–Ti magnet technology to its extreme. Design innovations were [26]: (i) use of the two-in-one design proposed first by BNL and dismissed for the SCC and RHIC; actually, the LHC went further by using for the dipole the original "twin" variant, where the two channels are fully coupled both magnetically and mechanically; (ii) cooling to 1.9 K to boost Nb–Ti performance and make use of the superior conductivity and heat transfer properties offered by superfluid helium. In fact, up to 1989 the use of Nb_3Sn was still considered, with R&D that was marked by the first break of the 10 T wall by a dipole coil [27]; however, cost and industrial maturity were in favor of Nb–Ti and HeII, and the performance of Nb_3Sn had to improve significantly over that of Nb–Ti, which happened only many years later, as shown in the graph of Fig. 16 and discussed in Ref. 10.

Another significant innovation of the LHC SCMs was in the control of the interstrand resistance of the cable. Also called contact resistance, R_c, this critical parameter that controls interstrand coupling currents was still an open point of the SSC design at its closure (at least for the SC booster); the large LHC cable is vulnerable to values below 10 $\mu\Omega$, while the high J_c calls for collective cable stabilization, which can disappear for values beyond 100–200 $\mu\Omega$. Interstrand resistance values in the right window, $10 < R_c < 200\,\mu\Omega$, were obtained by carefully

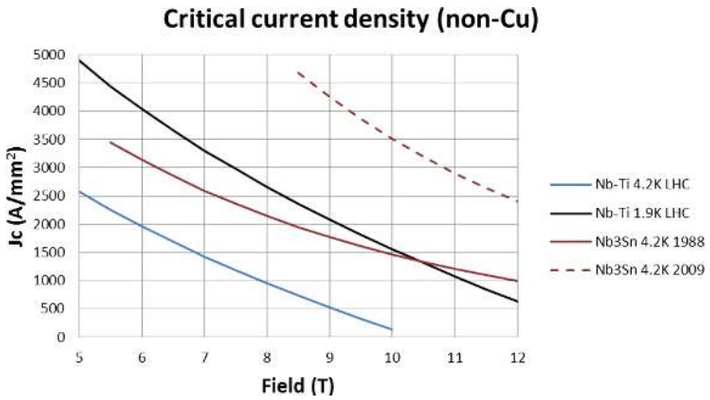

Fig. 16. Critical current density of Nb–Ti, at 4.2 and 1.9 K, compared with that of Nb_3Sn at 4.2 K, this last at the time of the LHC decision on superconductors and today.

controlling the thickness of the Sn–Ag coating layer of the strands, followed by a customized (according to actually measured thickness) air heat treatment of the whole cable to induce surface oxidation [28].

3.5.3. *LHC dipole magnet design*

The LHC main dipoles (or main bends, MBs) have been designed for a nominal operation at 8.33 T, 86% of the maximum current $I_{\max}$, or $l = 0.86$ (see Subsec. 2.2.4), which is the critical current on the load line. The mechanics was, however, designed for the "ultimate" field of 9 T, corresponding to $l = 0.93$.

The design of the LHC MBs has gone through about 10 years of evolution, with three generations of design, all featuring two coil layers wound with different cables [29]. The three generations differ in the coil layout, in the collar design and in how the coil–collar assembly interferes with the yoke-skin assembly. Making reference to Fig. 17, in which the details of a quadrant of one aperture are visible, the basic design characteristics of the third — final — generation are:

Coil layout. With a 56 mm free bore, it is based on six-conductor blocks. After an unsuccessful attempt in 1992–98 to work with five coil blocks of the second generation, the final design has been based on an optimized six-block layout, where the conductors are as radial as possible and the shear forces among conductors are minimized.

Coils. The two conductor shells are wound with different cables whose margins in critical current are very similar, so it is an optimized grading. This

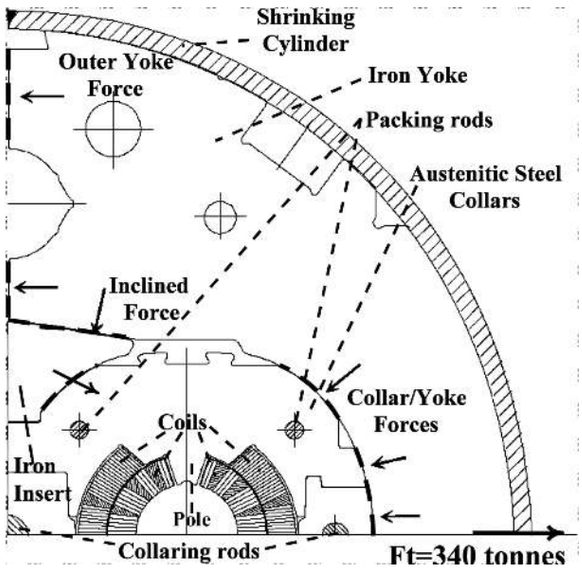

Fig. 17. Quadrant of the LHC dipole, with all mating surfaces indicated.

feature has improved the central field per unit current but has reduced the margin to quench, and it implies that imperfections in the winding of the second layer are as important as those of the inner layer, despite the considerable number of turns grouped in the two blocks of the outer shell.

The coils are composed of poles of two layers each. The necessity to avoid sorting in order not to slow the production requires that each pole, and even each layer, be identical within 100 μm, which corresponds to a variation of about 0.1% of the main field, 3.5 and -0.4 units (10^{-4}) of the main harmonics, sextupole and decapole respectively, and to

about 12 MPa in azimuthal coil prestress. The necessity of top–bottom and left–right symmetry means that coils must all be similar, even better than the stated figures.

Collars. These are of the twin type, i.e. the two magnetic channels are fully coupled, a novelty that was not without risk. Made out of special austenitic steel with very low magnetization under operating conditions, collars are obtained by fine blanking according to a shape that ensures the wanted coil cavity under stress and cold conditions, and for this reason the collars are slightly elliptical ($\varepsilon = 0.1$ mm) when punched. The choice of stainless steel was introduced relatively late in the Project, after a long period when an aluminum alloy was preferred. With the aluminum collar the prestress induced by thermal contraction would have been good for 5 T or so, like for HERA. The additional restraining was coming from the external shrinking cylinder through the yoke. For this reason the yoke had an open vertical gap; this gap and the weld-induced shrinking proved to be very difficult to control at the desired level of accuracy, especially in long magnets industrially built. The first long magnet of the LHC first generation, with six coil blocks [30], had aluminum collars and in 1994 reached 9 T in two quenches and no retraining; see Fig. 18. The approval of the LHC was based on that magnet; however, this success was not always reproduced by subsequent magnets. So, austenitic steel for collars was introduced as the last big modification, allowing for a more comfortable margin in the construction and assembly tolerances. Also, thanks to its higher rigidity, the use of austenitic steel helps limit (but cannot avoid) conductor movements, as discussed in Ref. 14.

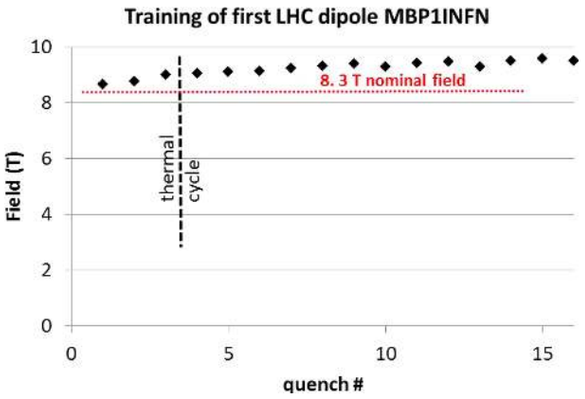

Fig. 18. Training quench of the first full prototype of the LHC dipole (CERN–INFN collaboration, 1994).

Iron. The presence of an iron insert at the vertical symmetry plane in between collar and iron yoke (see Fig. 17) helps the assembly accuracy and the transmission of vertical force from the shell to the collars, through the iron yoke, in a position that is critical for the twin design. Indeed, the lack of left-to-right symmetry in twin collars is one of the main disadvantages with respect to the single collaring coil assembly. The inclined surface of the iron insert is meant just to compensate for the reduced rigidity in the central arm of each aperture of the collars. The interference between the iron yoke and the collars is also situated at the midplane, the outer arm of each aperture, and at two different positions along the collar outer arm. The iron insert proved to be useful for fine-tuning the field quality for even harmonics.

Cold mass assembly. As previously stated, the coil–collar assembly is surrounded by the magnetic circuit contained by a shrinking cylinder, formed by welding two half-shells made out of austenitic steel. The carefully controlled welding shrinkage provides the necessary rigidity to the whole magnet. The forces are transmitted by interference among very rigid pieces (collars and yoke). Therefore, not only is the precision of the single pieces high (typically $\pm 20\,\mu$m for the collars and $\pm 50\,\mu$m for the yoke) but the assembly must ensure this precision as well over the 15 m magnet length.

The typical azimuthal stress history (at the coil–collars interface, near the pole region, at 90°; see Fig. 17) for the LHC dipoles is shown in Fig. 19, where there can be noted relatively low prestress after cool-down, about 20% of the peak stress seen by coils during manufacturing, maybe the least satisfactory feature of the LHC dipole structural design. Magnet-to-magnet variation can be easily of the order of 15–20%. One should also note that the upper limit of the magnet powering is not necessarily zero stress, which implies detachment of the coil from the pole: if the friction associated with the movement does not generate excessive heat, the magnet can indeed reach a field in the range of 9.5 T to 10 T, corresponding to $I_{\max}$, as some models and prototypes did. However, this usually occurs with many training quenches and the reproducibility of this result would

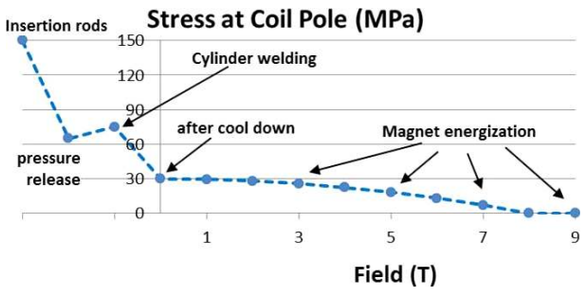

Fig. 19. Compressive stress at the coil–pole interface (see Fig. 17) for the LHC dipole during construction, cool-down and energization.

be very poor and not suitable for a reliable operating machine.

The magnet is curved, with a sagitta of about 9 mm, corresponding to a radius of curvature of 2812.36 m. This curvature has a tolerance of ± 1 mm, with the exception of the extremities of the magnet, where the tolerance is very tight: ± 0.3 (systematic) and 0.5 mm rms in order to keep the corrector magnets centered with respect to the beam tube, so as to avoid harmonic feed-down (detrimental to beam optics.)

3.5.4. *LHC main and insertion quadrupoles*

The main dipole system constitutes the backbone of the LHC and it alone accounts for 85% of the cost of the magnetic system, i.e. for almost 50% of the accelerator. The quadrupoles are of course the other main part of the magnet system, the last one being the corrector magnets, which will not be discussed in this article. There are various types of large quadrupoles: the main quadrupoles for a regular lattice and part of the dispersion suppressors, special quadrupoles for the rest of the dispersion suppressors, the matching sections between experimental regions and the regular arc, and the low-β quadrupoles just before the collision points.

The main quadrupoles (MQs) have been designed by the CEA–Saclay (France) team in collaboration with CERN [31]. The design was based on the same conductor as the main dipole outer layer, for cost and risk reduction — although, from the e.m. design point of view, the 15-mm-wide cable is really big for the 56 mm aperture of the magnet. For the same reason no grading was applied for the two layers, with some loss of design efficiency, but a gain in construction efficiency (use of the double pancake technique with no joint between the inner and the outer layer). The ratio of peak to useful field (λ; see Subsec. 2.2.4) is highly optimized. The magnet is a classical two-in-one, where the two coils are lodged in one iron yoke which has a central ridge — a central iron arm that magnetically decouples the two apertures. The forces are such that free-standing collars can comfortably retain the stress, the only coupling between collars and iron being the pins to insure straightness and proper alignment.

The matching section quadrupole (MQM) has many features similar to those of the MQ; however, the design was achieved with a much smaller cable, the objective being to reduce the powering current (6 kA, versus the 12 kA required by the MQ). Since all these magnets are individually powered [32], this choice greatly simplifies the cold powering. The coil "efficiency," i.e. the quantity of the superconductor for a given field/gradient, is higher than in the MQ. This is, however, at the expense of smaller margins for quench and stability.

Very interesting is the case of the MQY: these quadrupoles, also of classical two-in-one design with amperage of 6 kA or less, feature a large aperture — 70 mm. They operate at 4.2 K; however, thanks to grading of the superconductor in the two double layers and also to a special grading (the transition from the inner to the outer type of cable happens inside the second layer), they reach a peak field similar to the MQ and MQM (more than 6 T in operation, with 7.5 T as the magnet critical field) [32].

The low-β quadrupoles feature a single wide aperture of 70 mm and operate at 1.9 K. Here the two teams that shared the construction ended up with two very different designs. The Fermilab MQXB [33] was based on large cables (12 kA), with grading among the two layers, and free-standing collars inside

the iron yoke. The KEK MQXA [34] was based on small cables (7 kA) with four layers. The coils are assembled using 10-mm-wide spacer-type, nonsupporting collars. The prestress in the coils and their rigidity are provided by the yoke structure, which consists of horizontally split laminations keyed at the midplane. The locking of the yoke is similar to that of the collar for dipoles, so deviation from fourfold symmetry is a possible risk, which was finally successfully mastered. The MQXA design uses 40% more superconductor than the MQXB, and therefore has a higher peak field and gradient, which translate into a bigger margin, but it was possibly more complex to manufacture than the MQXB. Both designs proved to be successful and reached the goals, showing that optimization is not a rigid and unique concept.

A more detailed comparison of the e.m. design of these magnets, and others as well, can be found in Ref. 35; in Fig. 20 the cross section of the MQXA magnet is shown.

4. Experience from LHC Magnets

The LHC is such a large project with such a large number and so many types of accelerator magnets that the feedback from the construction and commissioning has great value for design and future projects.

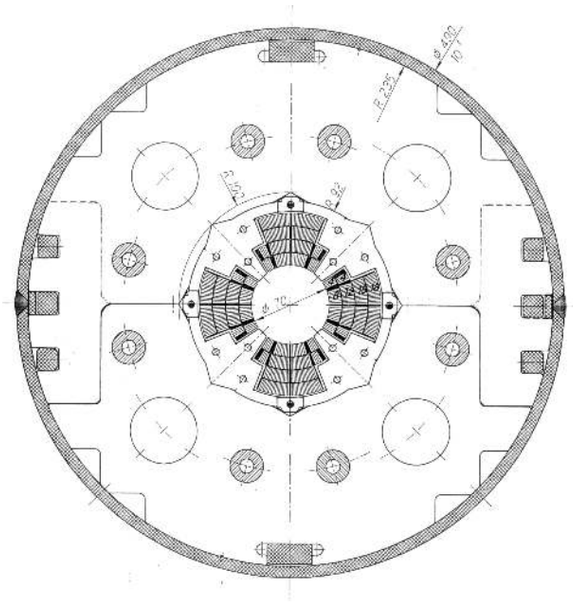

Fig. 20. Cross section of the MQXA, the low-β quadrupole designed by KEK in collaboration with CERN.

4.1. *Construction*

Design alone, good as it could be, cannot guarantee the accuracy and uniformity required of accelerator magnets: component construction and assembly are critical, too. The construction has been described elsewhere [36, 37], so here we recall that in the LHC the most important components that could influence the performance of the magnets, and that required uniformity all along the production, were kept under the control of CERN:

(i) All components of the coils from superconducting cables to copper spacers;
(ii) The main components of the 2D cross section: austenitic steel collars, iron yoke laminations, external cylinders;
(iii) Most mechanical components of the magnet, e.g. cold bore tube (beam pipe), HeII heat exchanger tube, end covers;
(iv) Most electrical components, e.g. quench heaters (for pre-series magnets), superconducting bus bars, protection diodes, instrumentation feedthrough.

All these components were designed and purchased by CERN separately and given to the magnet assemblers. In certain cases CERN even purchased the raw materials, which were then given to a company for transformation into finished components before delivery to magnet assemblers. This was the case when the properties of the raw materials were critical for performance: (a) the superconductor (Nb–Ti alloy) of the superconducting strands; (b) austenitic steel for collars; (c) low carbon steel (iron) of the yoke lamination.

In this way the risk of being "supplier of its own suppliers" was great and occasionally generated tension and organizational problems, and in a few cases some extra cost. However, in this way the final product was guaranteed and basically no surprises were experienced at the test and measurement of a magnet. Somehow CERN moved quality checks to the earliest possible moment, rather than waiting to check the final result and eventually rejecting what was not conforming. This was the key to the fact that all contracts for the main dipoles were completed according to the schedule, with negligible extra cost.

Since the coil is compressed in a cavity; given by the locked collars (see Figs. 14 and 17), the

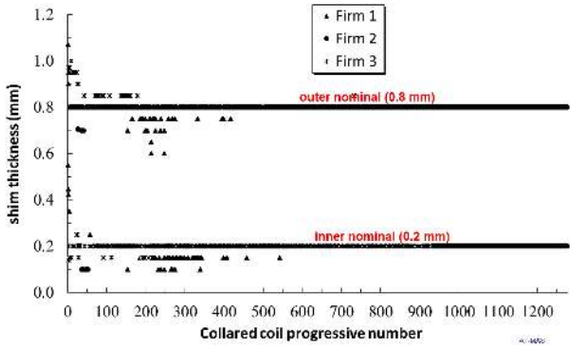

Fig. 21. Variation of the shim thickness for the two coil layers of LHC dipoles during manufacturing.

azimuthal prestress and the azimuthal length of the coils, this last determining the harmonic content, are not independent. As discussed earlier, the coil size determines the harmonic content. A 0.12 mm variation of the azimuthal length of the coil package (i.e. about 0.25% of the developed length) causes a variation of the sextupole b_3 of more than four units. On the other hand, if the coil is forced at a constant azimuthal dimension, the prestress at room temperature varies by 15 MPa. It was decided to steer production for field quality, i.e. the coil geometry was fixed irrespective of the induced stress variation, provided that the coil size — measured under 50 MPa stress — was not deviating by more than ± 0.12 mm. A larger variation triggered a fine-tuning of suitable shim positioned between coil upper end and pole; see Fig. 17. The shim variation from nominal size of the entire 1278-dipole production is reported in Fig. 21, from Ref. 38, where it can be noticed that adjustment was rare and mainly at the beginning. Variation of the coil's azimuthal length along the 15 m length of a similar coil was negligible, with $\sigma \sim 20\,\mu$m.

A key step in the quality control was the use of extensive magnetic measurements at low current, 8 A, at room temperature, carried out during construction on each magnet both as collared coil and then as "yoked" cold mass. Measurements were introduced first for steering production toward the field quality allowed window. This procedure triggered two fine-tunings of the cross section, done via change of the spacers inside the coil, to stay inside the target (see Fig. 22, from Ref. 38), where the results of the two interventions, carried out without stopping production, are clearly visible in the measured data. Dipoles with the first two cross sections were allocated almost all in one sector of the machine, compensating locally for the differences in the measured field components (see the next section).

In addition, the system proved to be a useful tool for detecting serious hidden defects that could impact on the magnet quench or electrical performance. Intercepting defects at the earliest stage, by any means, including complex magnetic measurements, has been a guiding star for the LHC project. Its usefulness also for correcting weak procedures, besides finding single large mistakes, is summarized in Fig. 23, where the number of coil disassemblies triggered by magnetic measurements on the production premises is plotted as a function of production. Mistakes were numerous at the beginning; then, after a quiet period when we thought that production was well under control, we had a sudden increase, and we

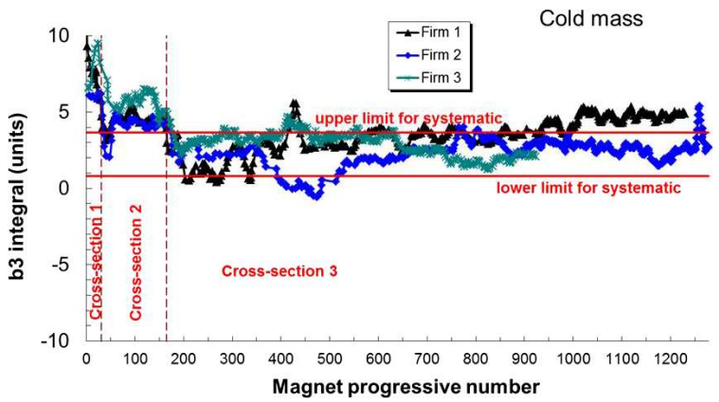

Fig. 22. Sextupole components of all dipoles measured at warm at the three manufacturing sites. The data on the left of the dashed vertical line are the first 30 dipoles with the cross section before the first fine-tuning (see text for details).

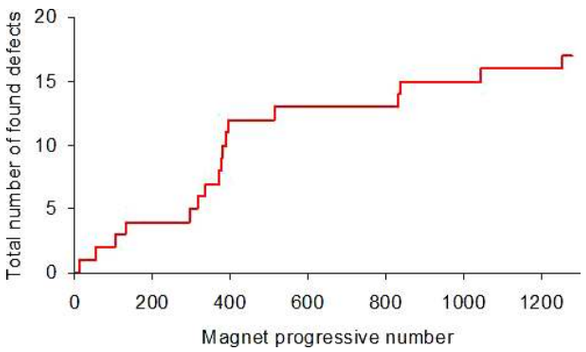

Fig. 23. Number of defects serious enough to trigger a coil disassembly during LHC dipole production.

were on the verge of blocking production. The sudden increase in the number of mistakes was correlated with massive injection of new personnel, necessary for reaching the required rate for mass production; review of procedures, tighter QA and careful training of personnel were among the remedies that eventually made the two-thirds remaining of production very stable, with very few deviations observed.

The production of the LHC magnets lasted seven years. Preseries contracts (7% of the total) were signed in 2000, series contracts in 2002, and the last dipole and quadrupole were delivered perfectly on time, on 7 November 2006. We had less than 2% of magnet rejections, and only two (less than 0.2%) could not be repaired. This success demonstrated the achieved maturity of the SCM technology based on Nb–Ti, eventually completing the route initiated by the Tevatron.

4.2. *Installation and sorting*

Well-performing magnets are a prerequisite for a good accelerator, but beam quality and reliable operation require additional considerations of sorting and optimal placement, as well as precise and reproducible control. This was done to a high degree for the LHC.

A total of approximately 1800 large SCMs had been produced, tested and installed during the four years of construction of the LHC. Each magnet was examined from the viewpoints of electrical performance, magnet protection, field quality and magnet alignment, by a Magnet Evaluation Board [39] charged with magnet acceptance and sorting for the whole ring. The installation and tunnel location of the magnets in the LHC accelerator were optimized

Table 4. Magnet sorting criteria.

Type of magnet	Number	Sorted quantity
Arc dipole (MB)	1232	Geometry Field (b_1, a_2, b_3) Training
Arc quadrupoles (SSS)	360	Field (b_2)
Dispersion suppressor quadrupoles	64	Training of trim quadrupoles Geometry
Matching sections quadrupoles	50	Geometry
Cold low-beta quadrupoles (Q1...Q3)	24	Geometry
Separation and recombination cold dipoles (D1...D4)	16	Geometry
Warm quadrupoles (MQW)	48	Field geometry

based on the magnet performance (mainly geometry and field quality, but also electrical and quench issues). The objective was to preserve and, if possible, optimize the machine performance as originally projected by the design studies. Sorting followed the criteria listed in Table 4.

Some of the motivations and results of sorting are shown by two representative plots in Figs. 24 and 25. In Fig. 24 we show the maximum deviation of the mechanical axis of the dipole for all magnets installed (two bores, V1 and V2), on top of the class definition for installation in the dispersion suppressor region (golden), any location in the arc (silver) and the middle of a regular cell (midcell). In spite of

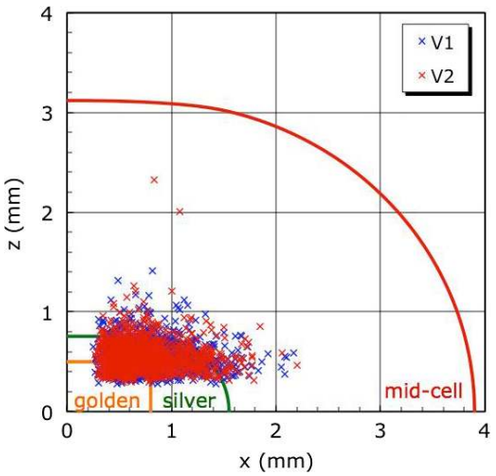

Fig. 24. Measurements of the geometry of the LHC main dipole and sorting class (see text for details).

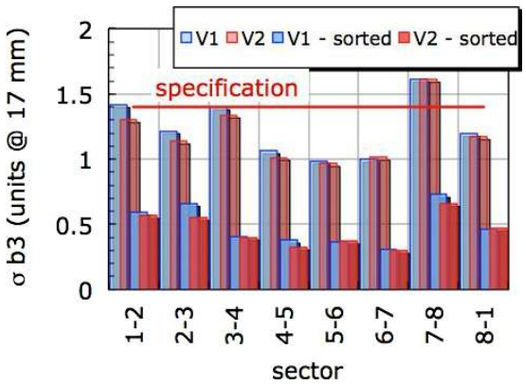

Fig. 25. Rms b_3 for the two beam tubes of the LHC: with no sorting (higher columns) and with sorting.

a significant fraction of magnets exceeding the manufacturing specification of 1 mm on the axis deviation from the nominal orbit, sorting of dipoles by their geometry has allowed us to preserve the accelerator mechanical aperture to values exceeding initial specifications, and with no bottleneck in the arc.

A similar benefit of sorting is observed in Fig. 25, where we plot the rms normal sextupole b_3 for the arcs of each of the eight sectors into which the LHC is subdivided, for both of the apertures V1 and V2. Two columns report rms b_3 as would be obtained by a random installation, and the two smaller columns represent its effective value when pairing and compensation are taken into account. Typically, the values of b_3 fall within the manufacturing specification, with a marginal exception for sector 78, which contained the initial production with a different cross section. After sorting, the effective rms b_3 is reduced by a factor of 3, with the benefit of a strong reduction of the third order resonance driving term.

4.3. *The 2008 incident*

On 19 September 2008, just nine days after the spectacular first circulating beam in the LHC, the magnet system experienced a very grave incident. During the current ramp-up of the last sector which was not yet brought to its maximum (indeed, start-up was done with two sectors not yet fully tested), a faulty electrical interconnection, carrying about 9 kA, melted away, generating an electric arc that perforated the helium vessel. There were many consequences, with huge collateral damage due to the helium pressure rise (above 8 bar, instead of the 1.5 bar of design). Consequently, 53 main magnets were removed and only 16 could be reinstalled after minor interventions; 37 magnets, a more than 500 m length of the accelerator, had to be replaced with spares, which were barely sufficient in number. The finding and recommendation can be found in Ref. 40, while detailed descriptions and considerations of the reasons have been discussed in Ref. 41. The incident was triggered by the only completely faulty interconnection (now we know this for sure); however, the electrical splice between magnets is done according to a weak design and even apparently good splices have a nonnegligible probability of undergoing a thermal runaway at high current because of discontinuity of the copper stabilizer. For this reason the accelerator performance is today limited to 60% in terms of the magnetic field and then of the beam energy. Only a campaign of consolidation, foreseen in 2013–14 and aimed at assuring stabilizer continuity in all splices and at fixing the defectives ones, will allow the LHC to reach its nominal design parameters.

It is, however, useful to comment that the incident happened because an interface was not given the necessary attention. Considered mainly as a mechanical problem, there was insufficient analysis of the superconducting behavior of the bus bar joints, which eventually resulted in lack of continuity of the stabilizer and in lack of diagnostic and consequent protection.

It is also interesting to note that the electrical arc alone would have seriously damaged the two adjacent magnets, with some important but not severe collateral damage (pollution of the beam pipe). What made the incident so grave was the lack of protection against a release of liquid into the warm cryostat that was ten times larger than expected in the considered fault scenario. The magnet, cryostat and cryogenic teams did not discuss the possible worst scenario together, in this way missing implementation of a few simple measures that would have greatly reduced the consequences.

The lesson is somehow simple and complex at the same time: while the "superconducting magnet" is by far the most complicated part, the magnetic system is the realm of complexity. System integration is much more than simply fitting the components: it is the discipline that makes a laboratory apparatus a working device. In the case of the LHC magnet system, the superconducting bus bars, and its joints, earlier considered an "easy" component, are actually

a critical one that, together with the protection diode and the coil quench heaters, will probably be a source of concern during all of the LHC life. System integration is a view that should be considered at the early stage of a project, and even discussed together with the project of the main components, especially when dealing with a phenomenally complex machine like the LHC.

It is also important to note that recovery was very fast: indeed, the huge work of repair and reinstallation was carried out in less than nine months.

In Fig. 26 one can see the LHC magnets installed in the tunnel.

4.4. *Operation*

4.4.1. *Magnetic model*

The installed magnets are presently operated by a complex control system that translates the desired optics into powering currents on a circuit-by-circuit basis. The key elements of this conversion are the circuit transfer functions, based on measured field quality data that have been parametrized and synthesized into simple but complete fitting functions that form the Field Description of the LHC (FiDeL) [42]. FiDeL is a much-evolved form of the Tevatron feedforward and of the RHIC magnetic model. It allows dispensing of the reference magnets originally planned for the LHC, as was done for HERA, with a nonnegligible saving of cost and logistics. In addition to the transfer functions, FiDeL provides a parametrization of the field errors in the main magnet circuits (dipoles and quadrupoles), which is used to forecast currents in correction circuits. The commissioning tests of FiDeL, during the first injections into the LHC, have shown that the field model has a predictive capability of better than 10 units on the integrated dipole field (0.1% in energy), better than 25 units on the integrated quadrupole gradient (0.2 units of tune), and better than 0.5 units on the integrated sextupole (20 units of chromaticity). These results, achieved blindly (i.e. without beam feedback), are quite spectacular. Trimming the model using the accumulated beam-based measurements, and adopting strict precycling procedures, has reduced the range for day-to-day operation by one order of magnitude. The experience from the operation of all previous SC accelerators has led to a very good understanding of a number of key issues, the most outstanding being chromaticity control and beta-beating [43]. The stability of the magnetic machine, also thanks to the carefully studied precycle, is one of the characteristics most appreciated by the operation crew and one of the key elements of the success of LHC operation.

Fig. 26. LHC magnets in the LHC tunnel during electrical checks: in blue are the main dipoles, while the U-shaped tube visible in the middle connects a quadrupole to the cryogenic line.

Chromaticity correction, which has puzzled operators at the Tevatron and plagued those at HERA, is now possible at the LHC to within the equivalent of a few units of chromaticity (i.e. a few ppm of the sextupole field error) to be compared to 10 units (1000 ppm) of the sextupole error generated by persistent current in the dipoles (see Fig. 14). This includes a practically lossless compensation for the infamous decay and snapback responsible for up to 30% beam loss at the Tevatron.

Beta-beating, an indicator of the goodness of the local optics, has been found in the range of 30–40% for the *bare* machine at injection (i.e. before corrections are applied). This becomes 10% at the end of the ramp to 4 TeV, i.e. within the extremely

tight beam specification. Local corrections reduce the above values to 5–10% at most throughout the ramp.

4.4.2. *Quench and powering*

Accelerator magnets exhibit training, i.e. they initially quench at a current level well below $I_{\max}$, defined in Subsec. 2.2.4, but at each successive current ramp they tend to improve the current level at which spontaneous quench occurs. Eventually, the quench *training* attains a plateau, at which point the quench current does not improve any longer, as shown in the training curve of Fig. 18. The plateau current is ideally $I_{\max}$. In practice, however, for accelerator magnets the quench plateau is frequently around $l \sim 90\%$. This is not surprising, recalling our discussion on margins and stability. On one hand, when approaching $I_{\max}$ the reduction of the temperature margin and the limited amount of stabilizer cause a strong reduction of the stability margin, vanishing at $l = 1$. At the same time, the spectrum of mechanical perturbations increases in amplitude as the field increases, also because the mechanical structure may be designed for an operation current smaller than $I_{\max}$ (as previously mentioned, the LHC dipole has been mechanically designed for the ultimate operation at 9 T, i.e. $l = 93\%$). After a full warm-up of the magnet, the training generally restarts, with a new cycle of training quenches. The *training memory* is defined as the difference between the level of the last quench before a thermal cycle and the level of the first quench after the thermal cycle. Good memory means little loss of quench level, of the order of 5% or less, like the one shown in Fig. 18. Bad memory is sometimes referred to as "detraining." All LHC magnets have been cold-tested, at the final acceptance test at CERN, which has allowed their mechanical and electrical integrity and their quench performance to be assessed [44]. The 1232 LHC dipoles required on average just one quench per magnet to go beyond the nominal operating field of 8.3 T, at 11,850 A. The quench tests (carried out directly at 1.9 K without a previous test at 4.2 K) are important not only to assess if a magnet reaches and passes the nominal operating field but also to train the magnet in such a way that once it is installed in the tunnel it should not require much retraining. Because of the small stability margin, the memory between thermal cycles is far from being assured, and so the initial test strategy was to push all magnets to the ultimate field of 9 T in the first training curve and submit to a thermal cycle and retraining curve only the magnets with sluggish training behavior (those that needed more than nine quenches to reach 9 T). After some initial delay, the rate of magnet delivery ramped up so fast that it was not possible to execute all the planned tests within the allocated time. The magnet test sequence was then redefined and as a consequence the majority of the magnets were tested only up to the nominal field of 8.4 T or quenched not more than twice before they attained 8.6 T.

Only about 10% of dipoles have been submitted to a thermal cycle, either for verification purposes or because they were underperforming with respect to the above criteria. For this sample, the number of quenches per magnet to reach the nominal field at the second thermal cycle dropped, as expected, to an average of 0.10–0.15. The quadrupoles, having lower e.m. forces and stored energy, and a larger margin than the dipoles, needed on average less than 0.5 training quenches per magnet to pass the nominal current level of 11,850 A, and their memory was found sufficient to assure practically zero quench below nominal current in a training performed after the thermal cycle.

During commissioning of the installed magnets, in summer 2008, we found that a family of dipoles presented a loss of memory higher than expected. In Fig. 27, the forecast of quenches in the tunnel based on the single acceptance tests is reported as a continuous curve for all three dipole families (each

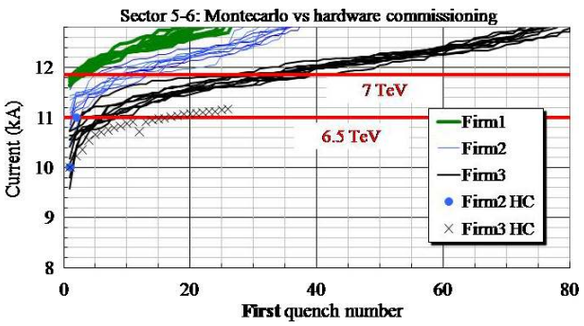

Fig. 27. Quench of LHC dipoles in the tunnel. Continuous curves represent the forecast based on the acceptance test, separated by manufacturer. Dot and cross markers are actual quenches that occurred during hardware commissioning (HC).

family corresponds to a different manufacturer); the spread in the curves indicates the uncertainty in the analysis. On the same plot, we report using dot and cross markers the quenches actually experienced during the commissioning campaign, before the start-up of the accelerator. Because of problems linked to the quench detection, the dipole current during commissioning was limited to the equivalent of 6.5 T (about 5.5 TeV in terms of beam energy). Out of the eight sectors, each comprising 154 dipoles, only one sector — sector 5–6 — was pushed up with the intention to reach nominal operation at 8.3 T. However, as can be noticed in Fig. 27, a number of quenches occurred, and the training slope is rather flat, more than expected from the extrapolation of data from series magnet tests. The training campaign of sector 5–6 was stopped at 7.9 T (6.6 TeV), because of the incident in sector 3–4, and it will be resumed only after interconnection consolidation in 2015; see Subsec. 4.3.

Sector 5–6 contains a predominance of firm 3 magnets, and for them a larger loss of memory was observed. It can be seen from the plot that the forecast for firm 3 (black curves) was slightly worse than for the other two families. It was, however, surprising to notice that the quenches during commissioning (indicated as "firm 3 HC" cross markers) stay consistently well below the corresponding forecast from the acceptance test at 1.9 K. For the moment the reason for this unexpected behavior is not known and no correlation could be reasonably established with factors that may have influence on training behavior. A study on this effect is reported in Ref. 45.

This effect, if confirmed, will probably require an estimated four months to train the whole LHC to reach 8.3 T, corresponding to the 7 TeV nominal beam energy. This is a tantalizing time, especially because there is no guarantee that the training memory will be retained upon a thermal cycle of an LHC sector. However, we also see that it should be very fast to reach a field corresponding to beam energies in the range of 6.5–6.7 TeV. This energy is short of the nominal goal, but should be a safe value to be reached rapidly after the 2013–14 shutdown. For a hadron collider the discovery potential is not a threshold function of the beam energy; the slight loss in terms of beam energy will be partly compensated for by more integrated luminosity, and hence is not a big issue.

5. Magnets for Pulsed Synchrotrons

The main challenge for fast-cycled accelerator magnets is not so much the bore field and aperture, which fall in the typical range of feasibility already demonstrated, but rather to achieve them with the required repetition rate, economically and reliably. A number of specific issues can be mentioned:

- *AC loss.* The control and reduction of AC loss in the cold mass has the utmost importance in reducing cryoplant investment and operation cost, and in limiting the temperature excursions in the conductor.
- *Cooling.* The heat loads on the magnet, especially those originating from the AC loss and beam heating, must be removed efficiently to warrant a margin sufficient for stable operation.
- *Quench detection and protection.* Protection of SCMs is especially demanding in the case of fast-ramping machines, due to the high inductive voltages in comparison with the voltage developed by a resistive transition. Voltage compensation and magnet protection must be proven in the presence of an inductive voltage during ramps that can be as large as 1000 times the detection threshold.
- *Field quality.* The contribution of coupling currents in the superconductor and eddy currents in the iron yoke is difficult to predict, control and measure at the desired resolution during fast ramps.
- *Material fatigue*, over several hundred million cycles, influencing material selection and, possibly, requiring dedicated testing.

An impulse to this line of research was given recently by the German laboratory GSI in Darmstadt, which is pursuing the construction of a new Facility for Antiprotons and Ion Research (FAIR) [46]. The central part of this complex is the two rings SIS100 and SIS300, which will be built in the same tunnel and will have magnetic rigidity $B_\rho = 100\,\mathrm{Tm}$ and $B_\rho = 300\,\mathrm{Tm}$, respectively. To achieve this magnetic rigidity, the dipoles of SIS100 will have a bore field of 2 T, with a window frame geometry mentioned in Subsec. 2.2.2 (see Fig. 8), providing a rectangular bore of 130 mm × 65 mm. The dipoles of SIS300 have a classical $\cos\vartheta$ layout, and they provide a peak field of 4.5 T in a round bore with a diameter of 100 mm. The magnets for these two rings are

especially challenging, because the operation mode of the complex foresees fast ramping of the energy. SIS100 should undergo a full cycle in 1 s, corresponding to a ramp rate of 4 T/s. The ramp rate requirements for SIS300, which will operate as a storage ring, are softer, but still the aim is to ramp the ring at 0.5 to 1 T/s.

The SIS100 R&D at GSI is supported by activities at the JINR laboratory in Dubna (Russia). A synchrotron similar to SIS100, the Nuclotron, has been in operation at JINR since 1994 [47]. The Nuclotron dipole magnets are operated in the accelerator at a peak field of 1.5 T, ramping at 0.6 T/s, and have achieved a peak field of 2 T, ramping at 4 T/s.

For SIS300, initial work has been performed in collaboration with BNL in the USA. At the time the accelerator had lower beam energy and dipole field requirements (it was actually named SIS200). A prototype magnet, GSI001 with a single layer coil and similar in construction to the RHIC dipole, was built and tested successfully at BNL, demonstrating operation up to a 4 T bore field in pulsed conditions up to 4 T/s. The magnet sustained short pulse sequences between 2 T/s (500 repeated cycles) and 4 T/s (3 repeated cycles) without quenching [48].

Since end-2006, the Italian INFN, in collaboration with GSI, has launched a prototype design and construction activity to demonstrate the feasibility and test the performance of a dipole for SIS300 [49]. The INFN program, dubbed DiSCoRaP, has focused on the design and construction of a dipole prototype with peak field of 4.5 T, curved with a sagitta of 28 mm over a 4 m length and with a ramp rate of 1 T/s, i.e. the present parameters for the SIS300 dipoles. The dipole (see Fig. 28) is at present under test.

An additional interest of the above R&D, beyond the construction of FAIR, is that the range of design parameters considered for SIS100 and SIS300 is the same as would be necessary for an upgrade of the PS and SPS injectors at CERN.

The range of parameters reported above is relatively large, and spans different technologies. We have nonetheless tried to find a common denominator among the various options by plotting in Fig. 29 the required field ramp rate (dB/dt) versus the peak field in the bore B. We notice an interesting feature of the scatter plot, namely that most of the points for fast-ramped magnets are clustered around a curve $B \times (dB/dt) = \text{const}$. In fact, the product $\Pi = B \times (dB/dt)$ is proportional to the power per unit volume released in the magnet. Hence, for a given magnet design, an increasing value of Π is associated with higher terminal voltage and AC loss, two of the main issues for ramped magnets listed

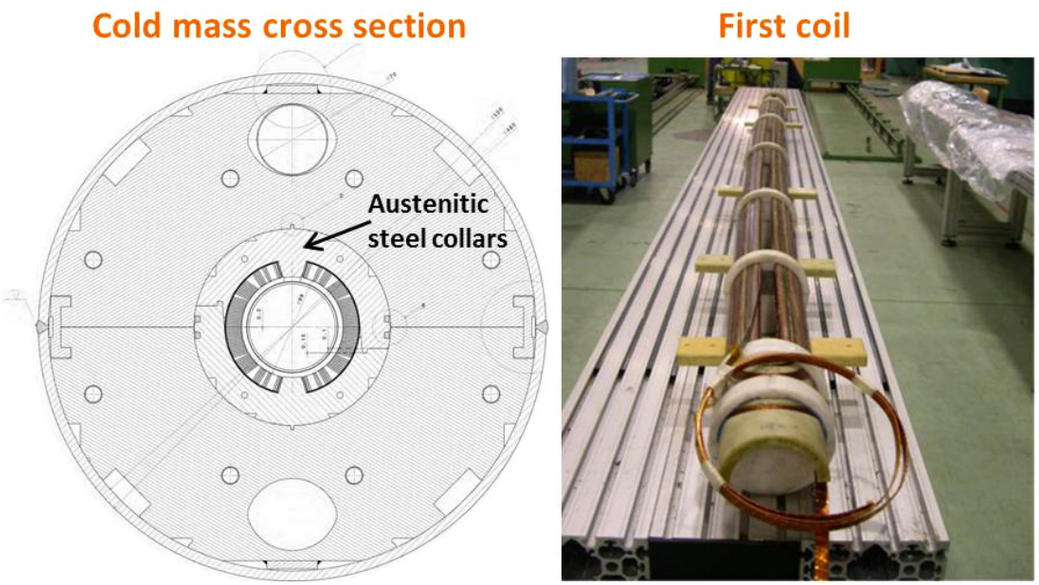

Fig. 28. Cross section of the cold mass and picture of the first curved coil of the DiSCoRaP dipole for FAIR-SIS300 (courtesy of G. Volpini, INFN–Milano).

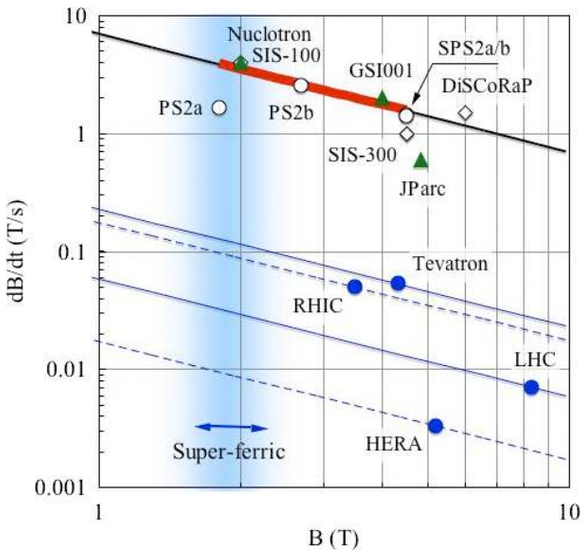

Fig. 29. *B–dB/dt* chart for SCMs: the ones for pulsed operation accumulate around the upper trend line.

earlier. Neglecting the large range of designs reported in Fig. 29, which is a conscious oversimplification, we can thus use Π as an indicator of the ramped performance: magnets with the same Π are assumed to be equally difficult to design and build, with respect to the pulsed mode. Most magnets presently in design or prototyping for ramped applications are aimed at a target value of $\Pi = 7\,\mathrm{T}^2/\mathrm{s}$, which also covers the range of parameters considered for both a PS and an SPS upgrade. The plot in Fig. 29 also reports the computed value of Π for the four large scale superconducting synchrotrons, to demonstrate the jump in performance sought after.

6. Next Generation High Field Magnets

6.1. *High luminosity LHC*

Although beam energy, which determines the discovery reach, is the first objective of a collider, luminosity, proportional to the instantaneous rate of collisions, is a very close second. Even more important is the time integral of the luminosity, i.e. the total number of collisions that can be recorded by the detectors. Once a collider has pushed the performance of the dipole magnets to its maximum practical limit, reaching the highest possible beam energy, the next, unavoidable step is to increase the luminosity, in order to improve the number and statistical relevance of the data from the detectors. If we take the example of the LHC, the collider presently operates at 4 TeV, which is approximately 60% of the nominal energy. The beam luminosity achieved so far is $0.7 \cdot L_0$, where L_0 is the nominal design luminosity, $L_0 = 10^{34} \cdot \mathrm{cm}^{-2} \cdot \mathrm{s}^{-1}$. This is an excellent result, considering that the planned increase in energy will yield additional luminosity. An indication of the good performance is the integrated luminosity (proportional to the total number of collisions), which amounts today to $15\,\mathrm{fb}^{-1}$ (inverse femtobarns), which is already more than the total accumulated during the seven years of Tevatron Run II. After the 2013–14 shutdown, when the main circuits splices will be consolidated (see Subsec. 4.3), the LHC is expected to reach an operating energy approaching the nominal 7 TeV. At this energy the luminosity will most likely exceed the nominal value L_0, thus further increasing the rate of data production. After a few more years, however, an increase in luminosity is required to further extend the physics reach of the collider. Indeed, around 2022 the present plan foresees carrying out an upgrade of the LHC to increase its peak luminosity by a factor of 5 and possibly multiply by a factor of 10 its integrated luminosity [50]. To reach this goal, at least two magnet systems, the collimation region and the low-β quadrupoles, will require a substantial upgrade, well beyond the limit of the present LHC technology. Especially for the low-β quadrupoles, the required performance is near the limit of the performance of Nb_3Sn (see Ref. 51 for a thorough discussion on limits of SC material for a high field). The work described above is within the scope of the broader High Luminosity LHC upgrade (HL-LHC). The High Luminosity machine is the next frontier for accelerator magnets: while the LHC has been the peak of 30 years of Nb–Ti magnet development, the HL-LHC gives the opportunity to prove on an existing accelerator the suitability of high field magnet technology, on a limited number of magnets. If successful, this could open the door to another, much bigger project based on SCMs.

6.1.1. *The 11 T two-in-one dipole*

The increased luminosity will require that additional collimators be placed in the dispersion suppressor (DS) region, which is at 1.9 K, to protect from the increased rate of particle loss. The DS region does

not have built-in space for the new collimators, which are 3–4 m long. One possibility of creating this space is to substitute a standard dipole ($8.3\,\mathrm{T} \times 14.3\,\mathrm{m} \cong 120\,\mathrm{Tm}$) with a dipole of equivalent integral bending strength, but producing a stronger field (11 T) over a shorter length (11 m). The bore field is well beyond the reach of Nb–Ti technology and therefore Nb_3Sn technology must be used for such magnets: Fermilab and CERN collaborate closely on this project.

Such a two-in-one dipole has many severe constraints. It must be powered in series with the other LHC main dipoles (i.e. the given operating current) and should be practically identical in bending strength (i.e. the given integral field) with harmonic content not too far from that of the LHC dipoles. In addition, the distance between the two apertures and the outer diameter of the cold mass must be the same as for a standard dipole (i.e. broad geometry fixed). The design adopted is a classical $\cos\vartheta$; see Ref. 52 and Fig. 30. The coil is based on cable built using a 0.7 mm strand with a minimum current density of $2750\,\mathrm{A/mm^2}$ at 12 T. The nominal copper content is 53% and the effective filament diameter is presently in the range of 40–50 μm.

The coil is double-layer, like the LHC dipole, but without superconductor grading, which would have required splicing between cables. The electromagnetic design is further complicated by two issues: (i) the superconducting persistent currents, due to high J_c and a relatively large filament size, generate a b_3 harmonic of ~ 45 units (10^{-4} of the main field) at the injection field, six times larger than that of the LHC main dipole; (ii) the 30% higher field in an iron yoke geometry that is essentially the same as for the LHC dipoles results in large saturation of the transfer function, and unacceptably high b_3 at the flat top field — 6.6 units.

Reduction of the persistent current sextupole can be obtained by means of passive magnetic shims near or in the coils. However, a further effort in reducing the filament size of the Nb_3Sn conductor from the present 50 μm to the range of 30 μm is pursued to bring the residual effect to within an acceptable range of correction of ± 10 units. The saturation effects are strongly reduced by shaping the internal iron profile and by a set of three saturation control holes — a well-known technique also used in the RHIC and LHC.

The mechanical design to withstand the forces, $\sim 70\%$ higher than in the LHC dipole, relies on clamping by austenitic steel collars and by a line-to-line fit between collars and iron yoke: the iron yoke and outer shell are assembled with interference, a procedure that avoids excessive stress during collaring but requires very tight tolerances and careful assembly. In this way the transverse stress, a constant concern with fragile Nb_3Sn, is kept below 150 MPa under all conditions, while the pole–coil interface remains always under compressive stress.

The plan for the LHC is to manufacture the 11-m-long dipole by joining in the same cryostat two straight magnets of length 5.5 m, placed such that the empty zone for the collimators is in the middle of the cryostat length. This configuration has the advantage that the equivalent kick is identical to that of a standard LHC dipole, without the need for further corrections. While the total number of

Fig. 30. Cross section of the 11 T two-in-one dipole and picture of the finished 2-m-long cold mass (single bore) ready for testing at Fermilab.

such dipoles is still under discussion, pending a better understanding of the present performance and future needs of the collimator system, the demonstration and prototyping works are in full swing. The plan foresees two short (~ 2 m) single bore dipoles, with the final cross section to be manufactured by end of 2012. The test of the first one is underway, with encouraging results. A full size, 5.5-m-long prototype is expected by 2015.

6.1.2. *The low-β quadrupoles and shell–bladder structure*

The keyword for the magnets needed for the upgrade in the collision region is "large aperture." The goal is to be able to further squeeze the beam in the interaction regions below the 55 cm nominal value of the betatron function at the interaction point (IP), the so-called β^*. The plan is to reduce β^* by a factor of 4, down to about 15 cm, so the aperture of the quadrupoles has to double from 70 mm to ~ 150 mm, the beam size being proportional to $(\beta^*)^{-1/2}$.

To keep the quadrupole triplet as compact as possible, the required gradient and the very large aperture result in high fields in the coil, in the range of 12 T. The baseline option is hence to procure Nb_3Sn quadrupoles. The technology is not yet fully validated for use in an accelerator, but remarkable progress has been achieved within the scope of the 10-year-long US-LARP[b] effort, through which several 90-mm-aperture quadrupoles and one 120-mm-aperture quadrupole have been built and tested in multiple variants and conditions.

In the first R&D phase, dealing with 1-m-long model magnets, two different mechanical designs have been pursued and evaluated: the classical collar-type structure and the so-called shell–bladder structure.

The shell–bladder structure, first developed for accelerator magnets at LBNL by S. Caspi [53], consists in precompressing the coils against an external restraining cylinder, or *shell*. We use the example of Fig. 31, where we consider for simplicity two racetrack coils, and substitute the collars with two thick plates, to illustrate the concept. *Bladders* in the interface between plate and iron yoke are pressurized to reach the final prestress plus an amount to compensate for spring-back. Permanent keys are inserted with minimal tolerance in slots between the plate and the yoke, after which the bladders are depressurized and removed. The coils are hence left in the desired situation of initial prestress. When the magnet is finally powered, the e.m. forces act on the coils, and release a portion of the prestress with ideally no movement of the coils; see Fig. 31. With respect to the classical collar system, the shell–bladder concept directly controls stress, rather than relying on the effect of interference between collar and coil. The prestress is thus less sensitive to the actual size and rigidity of the coil. In addition, since the cylinder can be in a material of high thermal contraction such as aluminum, there is the benefit of additional strain during cool-down. The latter effect can in principle be obtained also using aluminum collars (as in HERA and the early LHC design), but so far designers have

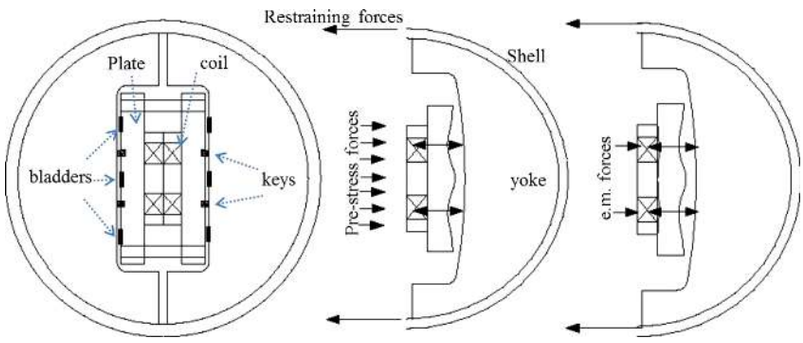

Fig. 31. Prestress based on the bladder-and-keys concept applied to a racetrack coil system.

[b]LARP (LHC Accelerator Research Program) is a US collaboration sponsored by DOE. The laboratories working on the LARP magnet R&D are BNL, Fermilab and LBNL.

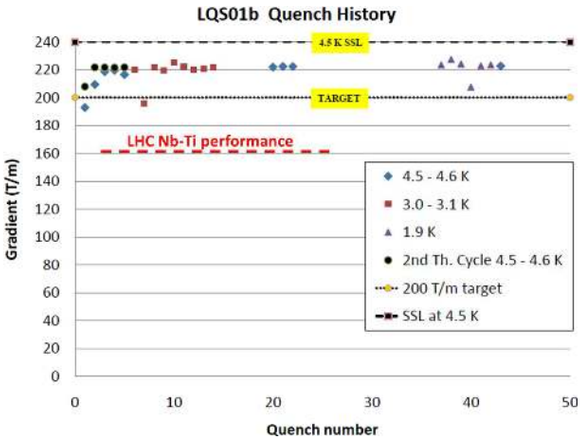

Fig. 32. Training curve of the Nb_3Sn LARP quadrupole LQS01b with the indicated equivalent Nb–Ti performance. The line indicated with SSL (short sample limit) is the magnet I_{max}.

considered impractical the use of aluminum collars for high field magnets.

The shell–bladder design has been so successful that in 2008 it was selected by the LARP collaboration as the baseline structure for the low-β quadrupole for the LHC upgrade, which at present is based on $\cos\vartheta$ layout. The successful test of the first "long" Nb_3Sn magnets — the so-called LQS, whose coils are 3.6 m long — has marked the definitive affirmation of this structure that has gone beyond expectation, attaining 90% of I_{max} with the version LQS01b [54]; see Fig. 32.

The structure is evolving further, adding features to assure alignment and field quality, with the design and construction of HQ, a 1-m-long model with a large coil aperture, of 120 mm — a further step toward the final requirement. Adding these features, which are now almost provided with a collar structure, makes the shell–bladder structure a little bit more complex (see Fig. 33), still retaining a few advantages with respect to collars. However, more designs and tests are necessary, especially in long magnets, before we can state that this shell–bladder structure constitutes a full alternative to collars for accelerator quality magnets.

The HQ quadrupole poses formidable challenges, given the jump in stresses and in stored energy per unit length. HQ has successfully reached 80% of its I_{max}, a threshold that is critical to qualifying a design for operation, and that for this quadrupole means a record 12 T peak field in the coils [55]. Nonetheless, a number of key issues, mainly of electrical insulation reliability, large strand and cable magnetization and repeatability of results, still need to be resolved.

For conductors, the target is J_c in the range of 1500 A/mm^2 at 15 T (for comparison, the ITER Nb_3Sn strand is based on J_c of 1000 A/mm^2 at 12 T, i.e. approximately 500 A/mm^2 at 15 T) and filament size of 50 μm or less. The two high current options (RRP from OST, USA; and PIT from Bruker, EAS, Germany) are both viable, with a clear advantage at this moment for the US product, which has benefitted from the long term conductor development program guided by DOE.

The main issues that still have to be resolved and on which the community is concentrating the effort are:

- *Performance.* Magnets still have to fully prove reliable operation at 80% of the short sample, and should be fully free from conductor instability.

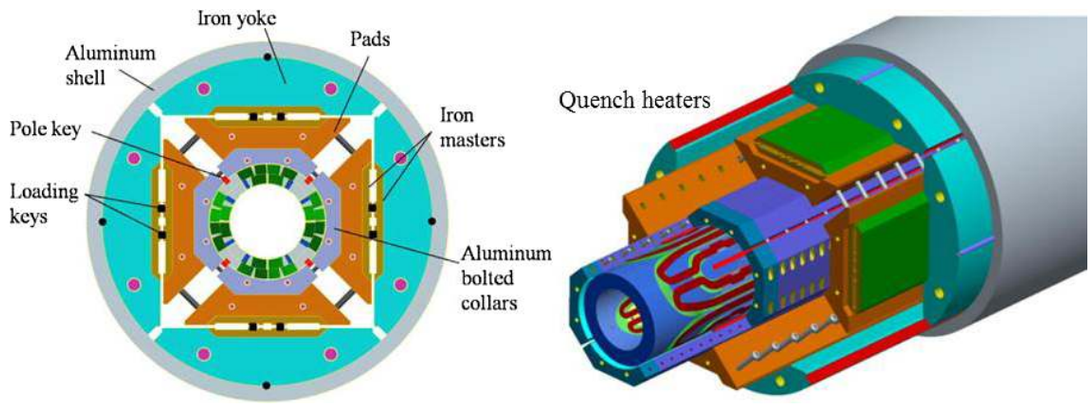

Fig. 33. Cross section and inside view of the LARP HQ quadrupole (courtesy of G. Sabbi, LBNL).

- *Field quality.* Coil geometry reproducibility, which is related to the random component of the field harmonics, although encouraging and improving, suffers still from poor statistics. A cored cable is almost certainly needed to avoid ramp rate effects due to the potential of low interstrand resistance, which can result from sintering. The next generation of LARP coils will make use of a cored cable, to gain experience on this issue, which is also relevant to the 11 T dipole project.
- *Radiation resistance.* All materials have to withstand an extremely high radiation load — to reach the final target of 3000 fb^{-1}, one has an accumulated dose that, in present estimates, could reach ∼10–100 MGy. A systematic program has been launched by CERN in collaboration with a few European institutes, as well as KEK and J-PARC in Japan.
- *Length.* With 150-mm-aperture magnets providing a 140 T/m operational gradient, the machine optics needs magnets of 7 m and 9 m length. So far, Nb_3Sn dipoles and quadrupoles exist as 1-m-long models, and a few 3.6-m-long quadrupoles. Replacing 9 m by two 4.5-m-long units is becoming the baseline, with moderate impact on luminosity performance.

6.2. *The high energy LHC and the HTS frontier*

The possibility of increasing the beam energy of the LHC has been considered at CERN in 2010 [56]. The project appears feasible; the most critical issue is the maximum field attainable by the main dipoles, which determines the final performance of the machine, according to (1).

The minimum goal of the high energy machine, the HE-LHC, is to double the present LHC design energy, but a more ambitious target has actually been set at 33 TeV of center-of-mass (collision) energy. A proton beam energy of 16.5 TeV requires operation of the main dipoles at 20 T, with a huge jump beyond the state of the art, as can be seen from the plot of the historical evolution of the dipole field for hadron colliders shown in Fig. 34, where the range of interest for the HL-LHC and HE-LHC is indicated, together with the domain accessible by various superconductors; see also Fig. 11.

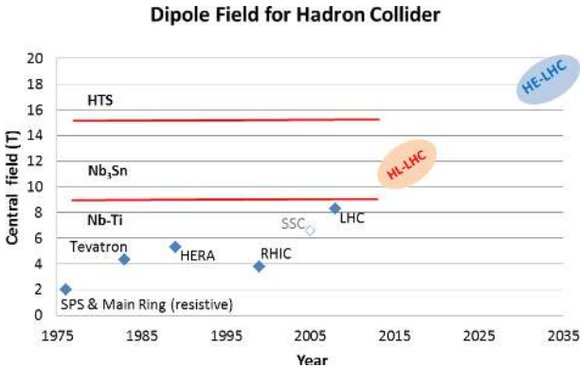

Fig. 34. Dipole field versus time for the main past projects and the region of interest for the LHC upgrades.

6.2.1. *Generic high field dipoles: R&D*

For high field magnets, the stresses are such that the shell–bladder concept previously mentioned looks very attractive. It can be applied to quadrupoles and dipoles, to $\cos\vartheta$ and to block coil layouts, i.e. to coils rectangular in shape, like the one in Fig. 31. The fact that Nb_3Sn coils have a very high modulus, more than 20 GPa rather than the 5–10 GPa common for NbTi, makes controlling stress via collars more difficult and favors the shell–bladder structure.

The quest for a high field dipole is at present underway via four main programs: (i) LBNL, with a long historical record, is pushing the limit of the rectangular block coil with the shell–bladder structure, with a series of magnets called HDs. HD2, which is the first to feature a free bore obtained with flare coil ends, (see Fig. 35), reached 13.8 T, which is about 78% of J_c [57], while HD3, with a larger bore, has experienced some electrical problems that are temporarily delaying the project; (2) the LD1 program — Large Dipole 1 — is a 13 T dipole with a large bore (> 100 mm) for a high field US cable test facility on the horizon of 2015; (3) the EU program EuCARD is aiming at producing first a large bore (> 100 mm) 13 T dipole, for the CERN cable test facility called Fresca2, by 2013, and then at reaching a total field of 19 T by adding a small HTS racetrack without a free bore; (4) the EU program EuCARD2 — just approved to start in 2013 — aims at developing a 10 kA class HTS cable and at designing and manufacturing a 5 T, 40 mm bore dipole of accelerator quality, wound with the cable mentioned above. The scope is to eventually insert the 5 T HTS

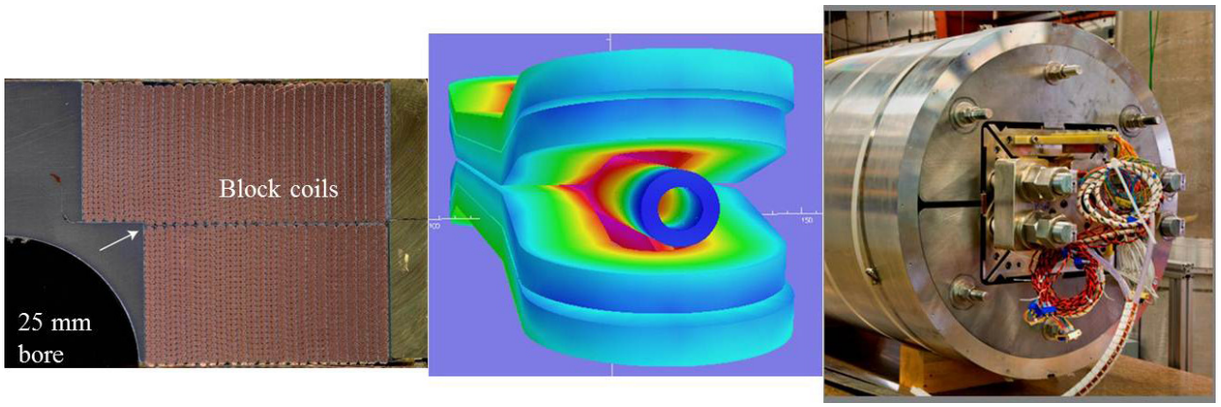

Fig. 35. HD2 dipole of LBNL: detail of the coil with arrow indicating a conductor displacement in the corner (*left*); FE model of the coil showing race-track structure with flare ends (*center*); picture of the cold mass before testing (*right*).

dipole into a large Nb_3Sn dipole to prove that HTS can enhance the field to > 15 T with a useful bore.

6.2.2. *Magnets for the collider: HE-LHC*

The possibility based on a dipole having an operating field of 24 T for an energy upgrade of the LHC was already considered in 2006 [58]. This was based, however, on a current density J_e of 600–800 A/mm^2 at 24 T, still far from being achievable. Recently, at CERN, a study has been carried out, and the target field for the main dipoles, the main driver of the entire project, has now been set to 20 T (operational) in a 40 mm bore, which would enable the HE-LHC to reach 33 TeV center-of-mass energy for proton collisions [59]. A prestudy clearly identified the following critical points:

- The required margin is set to about 20%, i.e. $l = 0.8$, which is large in absolute terms, being 5 T. The possibility of designing for a large l, and a lower margin, must be thoroughly investigated.
- The overall current density of the coil should be around 400 A/mm^2, at the design field, as it is for dipoles of previous accelerator magnets [60]. This requires that the engineering current density J_e of the basic element, strand or tape, be substantially higher than the overall 400 A/mm^2 in the operating coil. In order to generate 20 T in the bore, the coil width is about 80 mm, almost three times the width of the LHC coil.
- Bore size has been fixed at 40 mm, and the outer diameter of the iron flux return yoke must not exceed 800 mm (compared to 570 mm in the present LHC dipoles), which is a tough constraint considering the amount of magnetic flux that needs to be intercepted.

Based on previous observations, a preliminary magnet layout was designed, using Nb–Ti, Nb_3Sn and HTS conductor. Based on rectangular coil blocks (see Fig. 35), for its better suitability for shell–bladder force retention (anyway, given the size of the coil with respect to the bore, the gain of $\cos\vartheta$ versus block is negligible), it features an unprecedented superconductor grading, for cost reduction and volume containment, while gaining maximum performance. The possibility of separate powering of the coil sections is being considered. Although this configuration complicates the circuitry and the interconnections, it can offer us some key advantages:

- It allows separate optimization of cable size and amperage for the three materials. Moreover, while Nb–Ti and Nb_3Sn can be manufactured in very large cables (15–20 kA); this is not at all possible for HTS.
- Coil segmentation will favor magnet protection, a technique largely employed in the large solenoid magnets (working at ~ 1 kA rather than > 10 kA as accelerator magnets do), which is probably needed with an amount of stored energy and inductance ~ 15 times higher that of the LHC.
- Dynamic compensation of the field harmonics. This is extremely important, since it is very unlikely that Nb_3Sn and in HTS will feature the

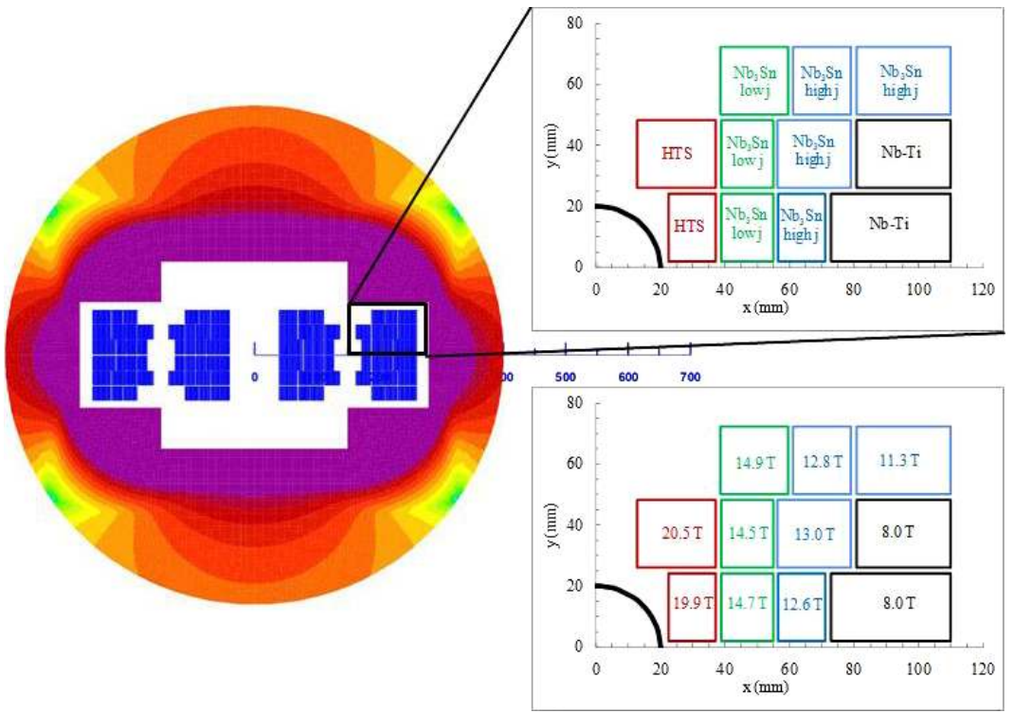

Fig. 36. Cross section of the preliminary magnet lay-out of the 20 T dipole for HE-LHC. The upper expanded quadrant shows the different superconductors used in each coil block, while the lower quadrant reports the peak field in each block.

5–7 μm filament size developed for the SSC and LHC Nb–Ti. We have to live with filaments in the range of 25–50 μm for Nb_3Sn, and most probably in the range of 50–100 μm for the HTS part, with sextupole components coming from persistent current of 50–100 units. Although the large ratio of coil width to bore size makes it easier to reach the necessary field quality, use of passive shims is unlikely to fully compensate for these large effects. Separate powering, first proposed for the SSC [61], would facilitate compensation of these effects as well as other dynamic effects due for example to interstrand resistance that are difficult to fully control at the cable level.

The project presents immense challenges, the first one being to make available the necessary superconductors and then to make them the required *conductors*. The total quantity of superconductor is three times that used for the LHC, i.e. about 3000 tonnes of finished strands (or tapes), containing about 40% of superconductor and 60% of stabilizer. Nb_3Sn certainly needs further improvement; however, it is on the good route, thanks to the HL-LHC–driven R&D. The biggest uncertainty concerns the HTS materials, which are still far from being ready for this type of practical application. The candidates are only Bi-2212 round wire, which has better 4.2 K transport properties than Bi-2223, and YBCO tape, whose performance is reported in Fig. 11.

Bi-2212 has the right topology for compact cables and possesses isotropic properties [62]. However, it has strong strain dependence, requires high temperature heat treatment in an O_2 atmosphere, and has been plagued, so far, by bubble formation and ceramic leakage through the silver barrier. Current density J_e is not far from the target; basically, we would need a moderate, but not modest, improvement of 50% over that of Fig. 11. Cost remains an issue, as well as little support from the rest of the superconducting magnet and conductor development community.

YBCO has the desired current density and it is mechanically robust. However, it is strongly anisotropic (see for example the two curves in Fig. 11), and is available only in the form of tapes.

Even ignoring the problem of magnetization, tapes are not suitable to be assembled in compact flat cable. Solutions like the Roebel bar and other types are under investigation. Indeed, one main aim of the above-mentioned EuCARD2 program is to address this issue, complementing the ongoing program in the USA, more focused on Bi-2212.

One issue, unfortunately equally shared by Bi-2212 and YBCO, is their very high cost: at least five times that of Nb_3Sn, which in turn is five times that of Nb–Ti. Any large scale high field magnet program is hence completely dependent on the success of the superconductor R&D and cost reduction program, in particular for HTS.

The basic R&D study on HTS for the HE-LHC must be carried out in the next 4–5 years, since by 2016 or 2017 a credible and substantiated design must be available. Should HTS not meet the very demanding requirements of the HE-LHC, the door to the 16–20 T region will be closed, at least for the objectives of the HE-LHC. The HE-LHC magnets will then be based on Nb–Ti and Nb_3Sn technology, with the goal being a maximum operating field of 15.5 T, a figure that still enables a respectable 26 T center-of-mass (collision) energy.

7. Conclusions

Accelerators are a fascinating domain for superconducting magnets because they constitute a very demanding application, with a spectrum of properties required for the magnets that are unmatched by other applications. We have limited our review to HEP accelerator magnets, which are by far more numerous and the ones where the technological advance is more evident: other types of accelerators require SCMs that are more similar in technology to solenoids and detector magnets.

For accelerator magnets, quench level is a critical issue, of course, but to enable their use in accelerators many other properties have to be controlled to a narrow window, simultaneously requiring a rigorous and integrated approach. The success of the technology and its enabling character is shown by the fact that four very large projects based on SCMs have been built in the last 30 years: Tevatron, HERA, RHIC and LHC. In this article we have discussed the continuation of the success story, namely the planned upgrades of the LHC and the first large pulsed synchrotron, FAIR, to be built at GSI. One key ingredient of the success is the capability of the accelerator community to provide a common forum for materials scientists, superconducting technologists and magnet engineers to discuss and to have mutual feedback. The global performance of an SCM — quench level, field quality, uniformity and reliability — depends in a decisive manner on the superconducting cable. New high field territory exploration critically depends on new materials — like HTS — growing from materials science to technical conductors. In a sentence: *A superconducting magnet cannot be better than its conductor — but it could be much worse*! *if not well designed, carefully manufactured and thoroughly tested.*

Acknowledgments

The authors thank Ezio Todesco of CERN for the fruitful discussions about magnet design, as well as for the material provided in the many years of analysis. The magnet scaling equations in Tables 1 and 2 are largely the fruit of the work of, and discussion with Paolo Ferracin of CERN.

References

[1] H. K. Onnes, Communication at the Third International Congress of Refrigeration (Chicago, Sep. 1913).

[2] Last Update in the Search for the Higgs Boson, seminar held at CERN, 4 July 2012; available at: https://indico.cern.ch/conferenceDisplay.py?confId=197461.

[3] R. A. Beth, Complex representation and computation of two-dimensional magnetic fields, *J. Appl. Phys.* **37**(7), 2568 (1966).

[4] I. I. Rabi, A method of producing uniform magnetic fields, *Rev. Sci. Instrum.* Vol. 5, Feb. 1934, pp. 78–79.

[5] E. Fischer, P. Schnizer *et al.*, Design and test status of the fast ramped superconducting SIS100 dipole magnet for FAIR, *IEEE Trans. Appl. Supercond.* **21**, 1844–1848 (2011).

[6] A. M. Akhmeteli, A. V. Gavrilin and W. S. Marshall, Superconducting and resistive tilted coil magnets for generation of high and uniform transverse magnetic field, *IEEE Trans. Appl. Supercond.* **15**, 1439–1443 (2005).

[7] L. Rossi and E. Todesco, Electromagnetic design of superconducting dipoles based on sector coils, *Phys. Rev. ST Accel. Beams* **10**, 112401 (2007).

[8] L. Rossi and E. Todesco, Electromagnetic efficiency of block design in superconducting dipoles, *IEEE Trans. Appl. Supercond.* **19**, 1186–1190 (2009).

[9] S. Caspi and P. Ferracin, Limits of Nb_3Sn accelerator magnets, in *Proc. 2005 Particle Accelerator Conference* (Knoxville, Tennessee), pp. 107–111.
[10] L. Bottura and A. Godeke, Superconducting materials and conductors, fabrication, and limiting parameters; this issue, 2012.
[11] M. N. Wilson, *Superconducting Magnets* (Oxford University Press, 1983).
[12] K. H. Mess, P. Schmuser and S. Wolf, *Superconducting Accelerator Magnets* (World Scientific, 1996).
[13] M. N. Wilson, NbTi superconductors with low ac loss: A review, *Cryogenics* **48**, 381–395 (2008).
[14] C. Lorin, P. P. Granieri and E. Todesco, Slip-stick mechanism in training the superconducting magnets in the Large Hadron Collider, *IEEE Trans. Appl. Supercond.* **21**, 3555–60 (2011).
[15] A. V. Tollestrup, Superconducting magnets, in *Physics of High Energy Accelerators*, eds. R. A. Carrigan, F. R. Hudson and M. Months (AIP Proceedings, 87, 1979), pp. 699–804.
[16] S. Wolff, Superconducting Hera magnets, *IEEE Trans. Magn.* **24**, 719–722 (1988).
[17] M. Anerella *et al.*, The RHIC magnet system, *Nucl. Instrum. Methods A* **499**, 280–315 (2003).
[18] A. Tollestrup and E. Todesco, The development of superconducting magnets for use in particle accelerators: from Tevatron to the LHC, in *Reviews of Accelerator Science and Technology*, eds. A. Chao and W. Chou, Vol. 11, pp. 185–210 (2008).
[19] M. A. Green, GESSS Machine Design Committee Reports, Report KFK 1764, 1972 (Kernforschungs Zentrum Karlsruhe).
[20] R. Perin, T. Tortschanoff and R. Wolff, Magnetic design of the superconducting quadrupole magnets for the ISR high luminosity insertion. Internal report CERN ISR-BOM 79-02, 1979.
[21] H. T. Edwards, The Tevatron energy doubler: A superconducting accelerator, *Annu. Rev. Nucl. Part. Sci.* **35**, 605–660 (1985).
[22] P. F. Dahl *et al.*, Superconducting magnet models for Isabelle, in *Proc. PAC 1973*, pp. 688–692.
[23] A. V. Zlobin, UNK superconducting magnets development, *Nucl. Instrum. Methods A* **333**, 196–203 (1993).
[24] C. Peters *et al.*, Use of tapered key collars in dipole models for the SSC, *IEEE Trans. Magn.* **24**, 820–822 (1988).
[25] J. Strait *et al.*, Tests of full scale SSC R&D dipole magnets, **25**, 1455–1458 (1989).
[26] R. Perin, The superconducting magnet system for the LHC, *IEEE Trans. Appl. Supercond.* **3** (1991).
[27] A. Asner, R. Perin, W. Wenger and F. Zerobin, First Nb3Sn superconducting dipole model magnets for the LHC break the 10 tesla field threshold, in *Proc. MT-11 Conference* (Tsukuba, 1989) (Elsevier Applied Science, 1990), pp. 36–41.
[28] D. Richter, J. D. Adam, D. Leroy and L. R. Oberli, Strand coating for the superconducting cables of the LHC main magnets, *IEEE Trans. Appl. Supercond.* **9**, 734–741 (1999).
[29] L. Rossi, The LHC main dipoles and quadrupoles toward series production, *IEEE Trans. Appl. Supercond.* **13**, 1221–1228 (2003); *errata corrige* in *IEEE Trans. Appl. Supercond.* **13**, 3874–3877 (2003).
[30] E. Acerbi, M. Bona, D. Leroy, R. Perin and L. Rossi, Development and fabrication of the first 10 m long, *IEEE Trans. Magn.* **30**, 1793–1796 (1994).
[31] M. Peyrot, J. M. Rifflet, F. Simon, P. Vedrine and T. Tortschanoff, Construction of the new prototype of main quadrupole cold masses for the arc short straight sections of LHC, *IEEE Trans. Appl. Supercond.* **10**, 170–173 (2000).
[32] R. Ostojic, The LHC insertion magnets, *IEEE Trans. Appl. Supercond.* **12**, 196–201 (2002).
[33] R. Bossert *et al.*, Test results from the LQXB quadrupole production program at Fermilab for the LHC interaction regions, *IEEE Trans. Appl. Supercond.* **14**, 187–190 (2004).
[34] Y. Ajima *et al.*, The MQXA quadrupoles for the LHC low-beta insertions, *Nucl. Instrum. Methods In Phys. Res. A*, **550**, 499–513 (2005).
[35] L. Rossi and E. Todesco, Electromagnetic design of superconducting quadrupoles, *Phys. Rev. ST Accel. Beams* **9**, 102401 (2006).
[36] L. Rossi, Experience with LHC magnets from prototyping to large-scale industrial production and integration, in *European Particle Accelerator Conference*, EPAC2004 118–122 (Jacow website), pp. 141–145.
[37] L. Rossi, The Large Hadron Collider and the role of superconductivity in one of the largest scientific enterprises, *IEEE Trans. Supercond.* **17**, 1005–1014 (2007).
[38] E. Todesco, Report on field quality in the main LHC dipoles, CERN report, EDMS No. 807803.
[39] P. Bestmann *et al.*, Magnet acceptance and allocation at the LHC Magnet Evaluation Board, in *Proc. PAC07* (Albuquerque, 2007), pp. 3739–3741.
[40] M. Bajko *et al.*, Report of the Task Force on the Incident of 19th September 2008 at the LHC, CERN LHC Project Report 1168, 31 Mar. 2009.
[41] L. Rossi, Superconductivity: Its role, its success and its setbacks in the Large Hadron Collider of CERN, *Supercond. Sci. Technol.* **23**, 034001 (2010).
[42] N. Sammut *et al.*, *Phys. Rev. ST Accel. Beams* **9**, 012402-1-12 (2006); **10**, 082802 (2007).
[43] E. Todesco *et al.*, The magnetic field model of the Large Hadron Collider: Overview of operation at 3.5 TeV and 4 TeV, in *Proc. IPAC 2012*, pp. 2194–2196.
[44] P. Pugnat and A. Siemko, Review of quench performance of LHC main superconducting magnets, *IEEE Trans. Appl. Supercond.* **17**, 1091–1096 (2007).
[45] C. Lorin, A. Siemko, E. Todesco and A. Verweij, Predicting the quench behavior of the LHC dipoles

during commissioning, *IEEE Trans. Appl. Supercond.* **20** (2010).
[46] P. Spiller *et al.*, Status of the Fair SIS100/300 Synchrotron design, in *Proc. PAC07* (Albuquerque, New Mexico), pp. 1419–1421.
[47] A. D. Kovalenko, Nuclotron: Status and future, in *Proc. EPAC 2000* (Vienna, Austria), pp. 554–556.
[48] G. Moritz *et al.*, Recent test results of the fast-pulsed 4 T $\cos\Theta$ dipole GSI001, in *Proc. 2005 Particle Accelerator Conference* (Knoxville, Tennessee).
[49] P. Fabbricatore *et al.*, Development of a curved fast ramped dipole for FAIR SIS300, *IEEE Trans. Appl. Supercond.* **18**, 232–235 (2008).
[50] L. Rossi, LHC upgrades plans: Options and strategy, presented at the *2011 Int. Particle Accelerator Conference*, *IPAC 2011* (San Sebastian, Spain), pp. 908–912.
[51] E. Todesco and P. Ferracin, Limits to high field magnets for particle accelerators, *IEEE Trans. Appl. Supercond.* **22**, (2012).
[52] A. Zlobin *et al.*, Status of a single-aperture 11 T Nb3Sn demonstrator dipole for LHC upgrades. Presented at the *2012 Int. Particle Accelerator Conference*, *IPAC 2012* (New Orleans, USA); published on the Jacow website.
[53] P. A. Bish, S. Caspi *et al.*, A new support structure for high field magnets. Lawrence Berkeley National Laboratory report, LBNL-47796SC-MAG 738.
[54] G. Ambrosio *et al.*, Progress in the long Nb3Sn quadrupole R&D by LARP, *IEEE Trans. Appl. Supercond.* **21**, 1858–1862.
[55] S. Caspi *et al.*, Test results of HQ01, a 120 mm bore LARP quadrupole magnet for the LHC luminosity, *IEEE Trans. Appl. Supercond.* **21**, 1854–1857 (2011).
[56] R. Assmann *et al.*, First thoughts on a higher-energy LHC, CERN-ATS-2010-177 (2010).
[57] P. Ferracin *et al.*, Assembly and test of HD2, a 36 mm bore high field Nb3Sn dipole magnet, *IEEE Trans. Appl. Supercond.* **19**, 1240–1243 (2009).
[58] P. McIntyre and A. Sattarov, On the feasibility of a tripler upgrade for the LHC, in *Proc. PAC'05*, pp. 634–636.
[59] E. Todesco and F. Zimmermann (eds.), The High-Energy Large Hadron Collider, Report CERN-2011-03 (2011).
[60] L. Rossi and E. Todesco, Conceptual design of 20 T dipoles for high-energy LHC, in *The High-Energy Large Hadron Collider*, report CERN-2011-03 (2011), pp. 13–19.
[61] F. R. Huson *et al.*, Superferric magnet option for the SSC, *IEEE Trans. Nucl. Sci.* **NS-32**, 3462–3465 (1985).
[62] A. Godeke *et al.*, Wind-and-react Bi-2212 coil development for accelerator magnets, *Supercond. Sci. Technol.* **23**, 034022 (2010).

Lucio Rossi obtained his PhD in physics from the University of Milan in 1980 and then started his researches on applied superconductivity for accelerators in 1981, at the University of Milan, where he became Professor of Experimental Physics in 1992. He worked on the Milan K800 Superconducting Cyclotron (5 T, 40 MJ), on the ZEUS detector thin superconducting solenoid for HERA at Desy, on the first superconducting dipole prototypes for the LHC, and on the 25-m-long superconducting toroidal magnet of the ATLAS experiment. In May 2001 Prof. Rossi joined CERN, where he led the construction of the superconductor and magnets of the LHC Project. Since 2011 he has been in charge of the High Luminosity LHC project and of the High Energy LHC study.

Luca Bottura is a Nuclear Engineer at the Engineering Faculty of the University of Bologna (Italy), and has received a PhD from the University College of Swansea (Wales, UK) for the physical modeling, scaling and numerical analysis of quench in large force-flow cooled superconducting coils. After nine years of experience in the design and testing of superconducting cables and magnets for fusion (NET and ITER), he joined CERN in 1995, where he initially supervised field mapping activities for the LHC magnets, and devised the Field Description for the LHC (FiDeL), an embedded system of the LHC controls. As of July 2011, he is the leader of the MSC group in the CERN Technology Department, in charge of the resistive and superconducting magnets for the CERN accelerator complex, the associated manufacturing and test technologies, and installations.